PLOS ONE

RESEARCH ARTICLE

Vaccinia virus-based vaccines confer protective immunity against SARS-CoV-2 virus in Syrian hamsters

Rakesh Kulkarni[1,2], Wen-Ching Chen[2], Ying Lee[2], Chi-Fei Kao[2], Shiu-Lok Hu[3], Hsiu-Hua Ma[4], Jia-Tsrong Jan[4], Chun-Che Liao[5], Jian-Jong Liang[5], Hui-Ying Ko[5], Cheng-Pu Sun[5], Yin-Shoiou Lin[5], Yu-Chiuan Wang[5,6], Sung-Chan Wei[2], Yi-Ling Lin[5,7], Che Ma[4], Yu-Chan Chao[2], Yu-Chi Chou[7], Wen Chang[1,2]*

1 Molecular and Cell Biology, Taiwan International Graduate Program, National Defense Medical Center, Academia Sinica and Graduate Institute of Life Science, Taipei, Taiwan, **2** Institute of Molecular Biology, Academia Sinica, Taipei, Taiwan, **3** Department of Pharmaceutics, University of Washington, Seattle, Washington, United States of America, **4** Genomics Research Center, Academia Sinica, Taipei, Taiwan, **5** Institute of Biomedical Sciences, Academia Sinica, Taipei, Taiwan, **6** Academi Sinica SPF Animal Facility, Academia Sinica, Taipei, Taiwan, **7** Biomedical Translation Research Center (BioTReC), Academia Sinica, Taipei, Taiwan

* mbwen@ccvax.sinica.edu.tw

Citation: Kulkarni R, Chen W-C, Lee Y, Kao C-F, Hu S-L, Ma H-H, et al. (2021) Vaccinia virus-based vaccines confer protective immunity against SARS-CoV-2 virus in Syrian hamsters. PLoS ONE 16(9): e0257191. https://doi.org/10.1371/journal.pone.0257191

Editor: Zhilong Yang, Texas A&M University, College Station, UNITED STATES

Received: August 4, 2021

Accepted: August 25, 2021

Published: September 9, 2021

Data Availability Statement: All relevant data are within the paper and its Supporting Information files.

Funding: The work is supported by grants from Academia Sinica, Ministry of Science and Technology, Taiwan (MoST109-3114-Y-001-001) to WC and NIH/NIAID (1R01AI129673) to SLH. The funders had no role in study design, data collection and analysis, decision to publish, or preparation of the manuscript. Website of Academia Sinica in Taiwan: https://www.sinica.edu.

Abstract

COVID-19 in humans is caused by Severe acute respiratory syndrome coronavirus-2 (SARS-CoV-2) that belongs to the beta family of coronaviruses. SARS-CoV-2 causes severe respiratory illness in 10–15% of infected individuals and mortality in 2–3%. Vaccines are urgently needed to prevent infection and to contain viral spread. Although several mRNA- and adenovirus-based vaccines are highly effective, their dependence on the "cold chain" transportation makes global vaccination a difficult task. In this context, a stable lyophilized vaccine may present certain advantages. Accordingly, establishing additional vaccine platforms remains vital to tackle SARS-CoV-2 and any future variants that may arise. Vaccinia virus (VACV) has been used to eradicate smallpox disease, and several attenuated viral strains with enhanced safety for human applications have been developed. We have generated two candidate SARS-CoV-2 vaccines based on two vaccinia viral strains, MVA and v-NY, that express full-length SARS-CoV-2 spike protein. Whereas MVA is growth-restricted in mammalian cells, the v-NY strain is replication-competent. We demonstrate that both candidate recombinant vaccines induce high titers of neutralizing antibodies in C57BL/6 mice vaccinated according to prime-boost regimens. Furthermore, our vaccination regimens generated T_H1-biased immune responses in mice. Most importantly, prime-boost vaccination of a Syrian hamster infection model with MVA-S and v-NY-S protected the hamsters against SARS-CoV-2 infection, supporting that these two vaccines are promising candidates for future development. Finally, our vaccination regimens generated neutralizing antibodies that partially cross-neutralized SARS-CoV-2 variants of concern.

tw/en Website of Ministry of Science and Technology, Taiwan: https://www.most.gov.tw/?l=en Website of NIH/NIAID: https://www.niaid.nih.gov.

Competing interests: The authors have declared that no competing interests exist.

Introduction

Severe acute respiratory syndrome coronavirus 2 (SARS-CoV-2), a member of the *Betacoronavirus* family, is causing a global pandemic and, as of July 2021, has infected more than 190 million people worldwide and resulted in 4 million deaths (https://covid19.who.int/) [1, 2]. Compared to two other highly pathogenic coronaviruses, SARS-CoV [3] and Middle east respiratory syndrome coronavirus (MERS-CoV) [4], SARS-CoV-2 has proven more difficult to contain [5]. Consequently, an effective vaccine to halt the spread of SARS-CoV-2 is urgently needed.

SARS-CoV-2 is an enveloped single-stranded positive-sense RNA virus, whose Spike protein (S) on the virion surface mediates virus entry into target cells [6–8]. Spike protein has S1 and S2 components and, similar to other type 1 viral fusion proteins, the S1 subunit contains a receptor-binding domain (RBD) that binds to its host cell receptor, angiotensin converting enzyme 2 (ACE2) [9], whereas the S2 subunit mediates membrane fusion [10]. The S protein of some SARS-CoV-2 strains requires cleavage by the cellular serine protease TMPRSS2 during cell entry [8, 11]. Neutralizing antibodies from convalescent patients recognize S protein, making it a good vaccine target [12, 13]. S protein is also a major target of T cell responses to SARS-CoV-2 [14, 15]. Although several SARS-CoV-2 vaccines, developed using mRNA technology [16–18] and adenovirus vectors [19–21], are currently in use; however, additional vaccines that are cost effective and could be transported without cold chain will still be worthwhile to develop. In addition, concerns have been raised of adverse effects following vaccination [22–24], implying that improvements to currently available SARS-CoV-2 vaccines are essential and will necessitate ongoing vaccine development.

Vaccinia virus has been deployed successfully to eradicate smallpox worldwide [25, 26]. The Modified Vaccinia Ankara (MVA) strain is growth-restricted in mammalian cells and preclinical and clinical trials have demonstrated it to be quite a safe vaccine vector against viral diseases such as HIV, MERS-CoV and SARS-CoV [27–30]. However, other attenuated strains of vaccinia virus exhibiting different degrees of immunogenicity could also serve as vaccine vectors [31–40]. Recently, several reports revealed that the MVA strain expressing SARS-CoV-2 S protein protected ACE2-transgenic mice and macaques from SARS-CoV-2 challenges [41–43]. Here, we generated SARS-CoV-2 vaccines using the MVA strain, as well as a v-NY strain previously employed as a vector for the first recombinant vaccinia virus (HIVAC-1e) used in FDA-approved clinical trials [44–48], both of which we engineered to express SARS-CoV-2 S protein. Unlike MVA, the v-NY strain is a replication-competent virus derived from the New York City Board of Health viral strain of smallpox vaccine [44–47] that displays reduced virulence compared to the standard smallpox vaccine (Dryvax). Due to the different features of these two vaccinia virus strains, we tested different prime-boost combinations of both vaccines to establish an effective regimen for immunoactivation in C57BL/6 mice. Furthermore, we demonstrate that our vaccination regimens generated antibody and T cell responses in mice and protected Syrian hamsters from SARS-CoV-2 infection.

Results

Generation of recombinant v-NY-S and MVA-S viruses expressing full-length SARS-CoV-2 S protein

The recombinant vaccinia viruses MVA-S and v-NY-S were generated by inserting an ORF encoding full-length SARS-CoV-2 S protein (Wuhan-Hu-1, NC_045512) into the *tk* locus of the vaccinia virus strains MVA and v-NY, respectively (Fig 1A). Cells infected with MVA-S and v-NY-S expressed high levels of SARS-CoV-2 S protein on cell surfaces, as revealed by flow cytometry (Fig 1B) and immunofluorescence microscopy (Fig 1C) analyses. Both full-

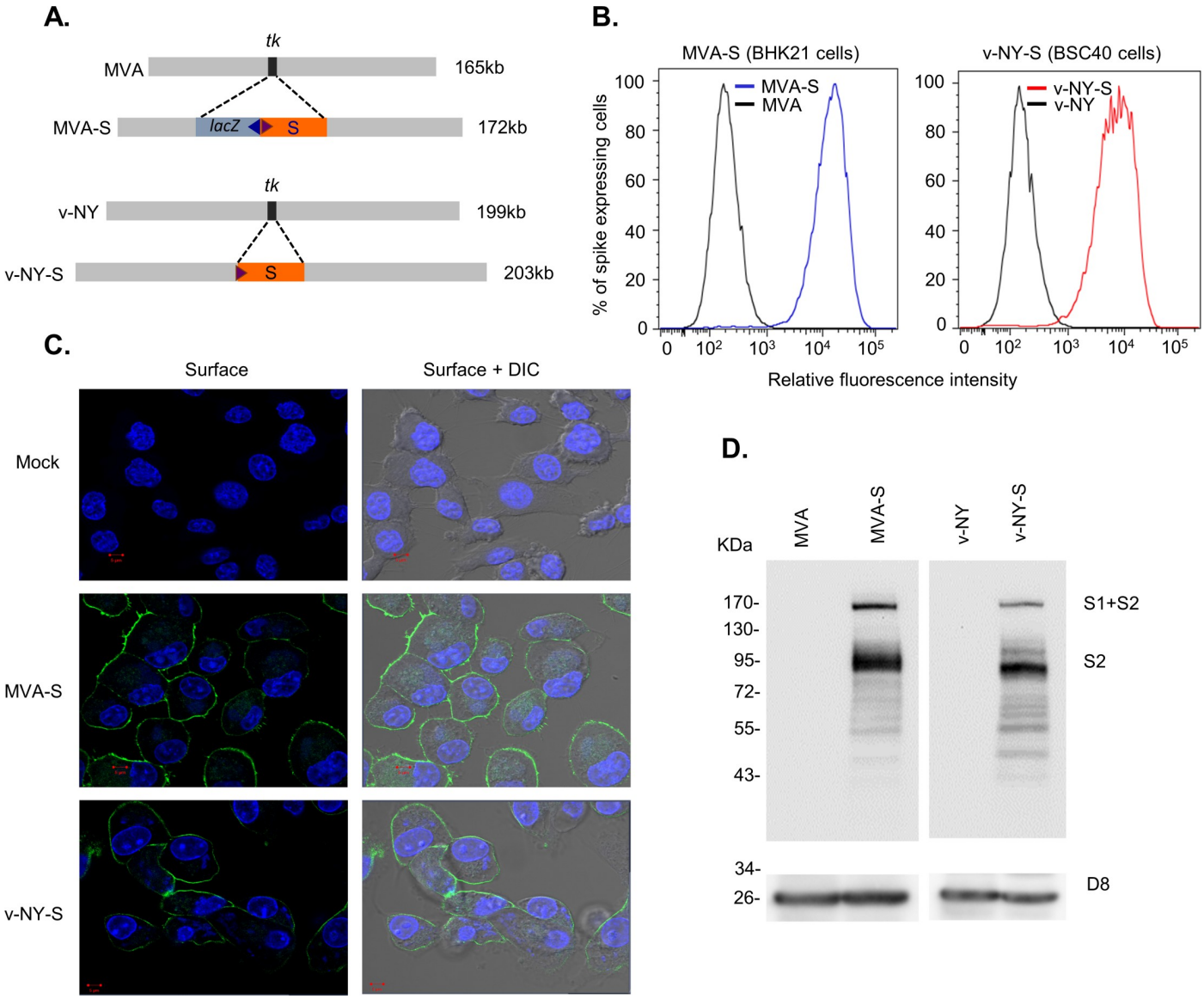

Fig 1. Generation and characterization of v-NY-S and MVA-S. (A). Schematic representation of the *tk* locus in the viral genomes of MVA-S and v-NY-S. The red box represents the ORF encoding SARS-CoV-2 S protein and the blue box represents the *lacZ* ORF. The small triangles represent viral promoters that drive gene transcription **(B).** Surface detection of SARS-CoV-2 S protein expressed from MVA-S and v-NY-S. BHK21 and BSC40 cells were infected with MVA-S (blue line) or v-NY-S (red line), respectively, harvested at 12 hours post-infection (hpi), stained with anti-RBD antibody, and then analyzed by flow cytometry. **(C).** Immunofluorescence staining of SARS-CoV-2 S protein in cells infected with MVA-S and v-NY-S. BHK21 and BSC40 cells were infected with MVA-S or v-NY-S at an MOI of 5 and fixed at 12 hpi with 4% paraformaldehyde, stained with anti-RBD antibody (green), and then photographed. Cell nuclei were stained with DAPI (blue). **(D).** Immunoblot of SARS-CoV-2 S protein expressed by MVA-S and v-NY-S. BHK21 cells were infected with MVA or MVA-S; BSC40 cells were infected with v-NY or v-NY-S, respectively, and harvested at 12 hpi for immunoblot analyses with anti-S2 antibody. Vaccinia D8 protein was used as a control.

https://doi.org/10.1371/journal.pone.0257191.g001

length and processed forms of S protein were detected in immunoblots (Fig 1D), confirming that the MVA-S and v-NY-S viruses stably expressed and processed SARS-CoV-2 S protein.

v-NY-S and MVA-S prime-boost vaccination regimens generate neutralizing antibodies in immunized C57BL/6 mice

We designed three prime-boost vaccination regimens using MVA-S and v-NY-S viruses (Fig 2A). Control mice were primed and boosted with PBS buffer alone. For the first regimen,

(MVA5/MVA1), mice were primed i.m. with $5x10^7$ PFU/animal of MVA-S virus and boosted with $1x10^7$ PFU/animal of MVA-S. For the second regimen, (vNY1/MVA1), mice were primed with $1x10^7$ PFU/animal of v-NY-S by means of tail scarification (t.s.) and then boosted i.m. with $1x10^7$ PFU/animal of MVA-S. For the third regimen, (vNY5/MVA1), mice were primed with v-NY-S at a higher titer of $5x10^7$ PFU/mouse by t.s. and then boosted i.m. with $1x10^7$ PFU/animal of MVA-S. For each regimen, the mice were primed at day 0 and primary (1˚) sera were collected 4 weeks later. These mice were then rested for 3 days, boosted, and then secondary (2˚) sera were drawn 2 weeks later. In some experiments, spleens were harvested 4 weeks after boosting for T cell and cytokine analyses. The t.s. site of vaccinated mice healed well and the mice remained healthy without any loss of body weight (S1 Fig). 1˚ and 2˚ sera were collected from mice and flow cytometry revealed that they recognized SARS-CoV-2 S protein expressed from recombinant S-BAC baculovirus (Fig 2B). Quantification (Fig 2C) confirmed that anti-spike antibodies were specifically generated after primary immunization and that antibody titers were significantly enhanced after vaccine boosting. Mice primed with v-NY-S presented higher levels of anti-spike antibody compared to those primed with MVA-S (Fig 2C). Immunoblot analyses (Fig 2D) also revealed anti-spike antibody reactivity to recombinant S protein, consistent with our FACS data (Fig 2C). We tested the neutralizing activity of 2˚ sera using SARS-CoV-2 spike pseudotyped virus (Fig 2E, panel i) and SARS-CoV-2 virus (Fig 2E, panel ii). Neutralization activity is presented as the reciprocal dilution of serum required for 50% inhibition of virus infection (ND_{50}). Our results show that all three regimens successfully generated high titers of neutralizing antibodies that inhibited SARS-CoV-2 S protein-mediated virus entry in both infection systems. Finally, we tested if our prime-boost vaccination regimens induced long-lasting antibody responses by comparing mouse sera collected at 0.5 and 4.5 months after the MVA5/MVA1 and vNY1/MVA1 regimens. Sera taken 4.5 months after boosting still contained 60–80% of spike-specific antibodies, as revealed by FACS analyses (Fig 2F), and a pseudotyped SARS-CoV-2 virus infection assay demonstrated that they retained comparable neutralization activity to sera at 0.5 months (Fig 2G), indicating these two vaccination regimens can elicit long-lived anti-spike antibody responses that have been shown to correlate with protection against SARS-CoV-2.

v-NY-S and MVA-S immunization generates a T_H1-biased immune response in mice

IFN-γ-producing T_H1 cells promote a B-cell class switch towards IgG2a/IgG2c, whereas IL-4-producing T_H2 cells promote a class switch towards IgG1 [49, 50]. Therefore, a ratio of IgG2c (or IgG2a) to IgG1 >1 is a good indicator of a T_H1-biased immune response, which is important for pathogen clearance. Accordingly, we used ELISA to measure levels of the IgG2c and IgG1 isotypes of anti-spike antibodies in C57BL/6 mouse sera collected after vaccination regimens (Fig 3A). All three vaccination regimens induced production of the IgG2c and IgG1 isotypes (Fig 3A) and with IgG2c/IgG1 ratios > 1 (Fig 3B), suggesting they had elicited a T_H1-biased immune response. We further *in vitro*-stimulated splenocytes from vaccinated mice with a SARS-CoV-2 spike peptide pool and then counted cells secreting T_H1 cytokines (IL−2, IFN-γ and TNF-α) and T_H2 cytokines (IL-4 and IL-6) (Fig 3C) [51, 52]. Consistently, we found that more cells secreted TNF-α and IFN-γ than IL-4 and IL-6 (Fig 3C), supporting that our three vaccination regimens triggered a T_H1-biased response [51, 52]. Furthermore, we investigated if our immunization regimens generated T effector memory (Tem) cells that are known to play a critical role in immune protection against secondary viral infections in lung tissue [53]. Splenocytes isolated from mice 4 weeks after vaccination regimens were incubated with a SARS-CoV-2 spike peptide pool for 2 h and then analyzed by flow cytometry (Fig 3D &

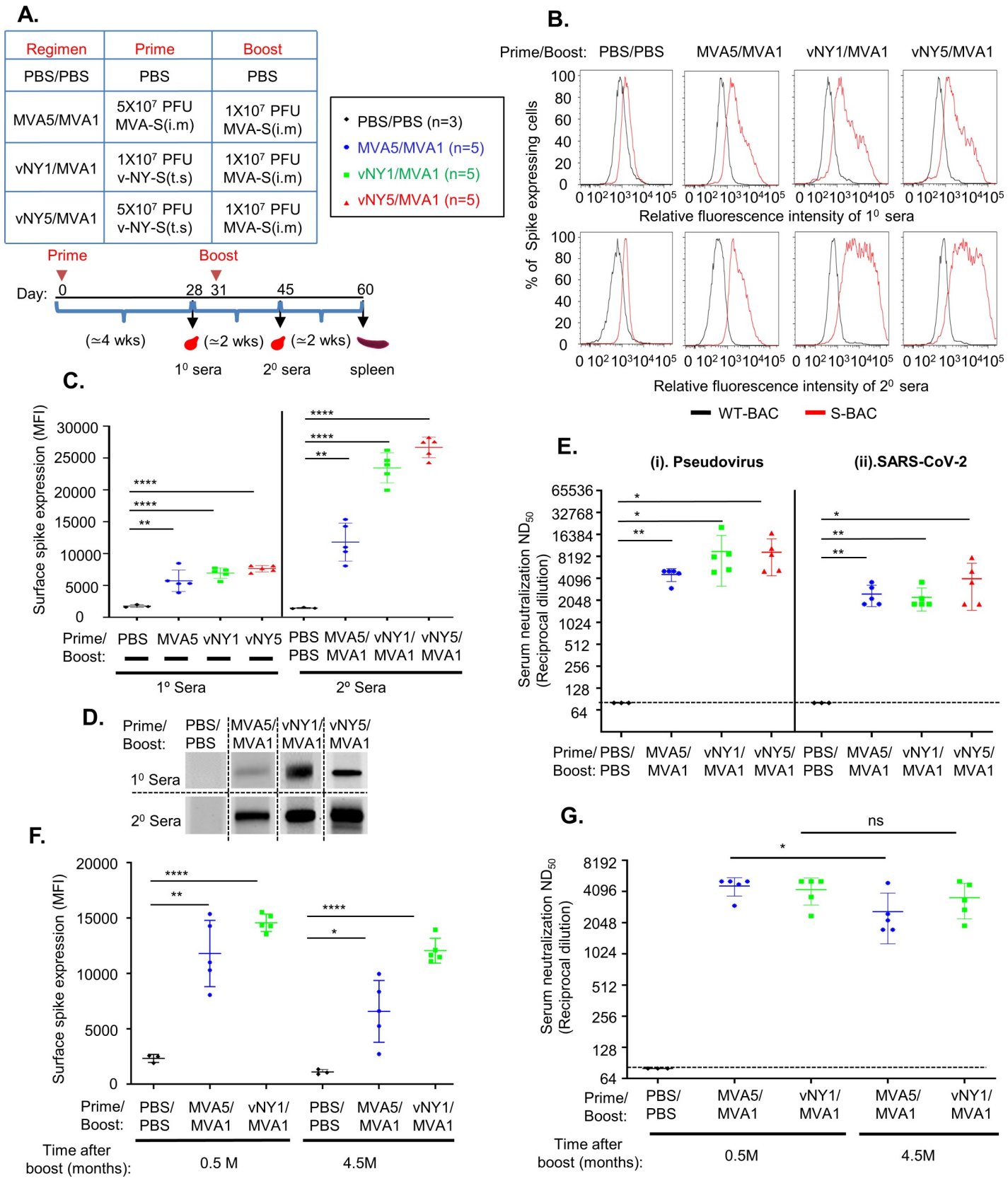
A.
Regimen | Prime | Boost
PBS/PBS | PBS | PBS
MVA5/MVA1 | 5X10^7 PFU MVA-S(i.m) | 1X10^7 PFU MVA-S(i.m)
vNY1/MVA1 | 1X10^7 PFU v-NY-S(t.s) | 1X10^7 PFU MVA-S(i.m)
vNY5/MVA1 | 5X10^7 PFU v-NY-S(t.s) | 1X10^7 PFU MVA-S(i.m)
PBS/PBS (n=3)
MVA5/MVA1 (n=5)
vNY1/MVA1 (n=5)
vNY5/MVA1 (n=5)
Prime
Boost
Day: 0 28 31 45 60
(≃4 wks)
(≃2 wks)
(≃2 wks)
1⁰ sera
2⁰ sera
spleen
B.
Prime/Boost: PBS/PBS MVA5/MVA1 vNY1/MVA1 vNY5/MVA1
% of Spike expressing cells
Relative fluorescence intensity of 1⁰ sera
Relative fluorescence intensity of 2⁰ sera
WT-BAC
S-BAC
C.
Surface spike expression (MFI)
Prime/ Boost:
PBS MVA5 vNY1 vNY5
PBS MVA5/ MVA1 vNY1/ MVA1 vNY5/ MVA1
1° Sera
2° Sera
D.
Prime/ Boost:
PBS/ PBS
MVA5/ MVA1
vNY1/ MVA1
vNY5/ MVA1
1⁰ Sera
2⁰ Sera
E.
(i). Pseudovirus
(ii).SARS-CoV-2
Serum neutralization ND50 (Reciprocal dilution)
Prime/ Boost:
PBS/ PBS
MVA5/ MVA1
vNY1/ MVA1
vNY5/ MVA1
F.
Surface spike expression (MFI)
Prime/ Boost:
PBS/ PBS
MVA5/ MVA1
vNY1/ MVA1
Time after boost (months):
0.5 M
4.5M
G.
ns
Serum neutralization ND50 (Reciprocal dilution)
Prime/ Boost:
PBS/ PBS
MVA5/ MVA1
vNY1/ MVA1
Time after boost (months):
0.5M
4.5M

Fig 2. Prime-boost MVA5/MVA1, vNY1/MVA 1and vNY5/MVA1 vaccination regimens elicited SARS-CoV-2 S protein-specific neutralizing antibodies in C57BL/6 mice. (A). Summary and timeline of the three prime-boost vaccination regimens and analyses. (B). Primary and secondary sera from immunized mice recognized SARS-CoV-2 S protein on cell surfaces. Mouse sera collected 4 weeks after priming (1˚ sera) and 2 weeks after boosting (2˚ sera) were assessed for SARS-CoV-2-specific IgG antibodies by flow cytometry using SF9 cells infected with either S-BAC (red line) or WT-BAC (black line). A single representative serum is shown in each histogram. (C). Quantification of anti-spike antibody titers in 1˚ and 2˚ sera from mice (as shown in B) using the mean fluorescence intensity (MFI) value from FACS. Numbers of mice for 1˚ and 2˚ sera collection are identical: PBS vs. PBS/PBS control (n = 3); MVA5 vs. MVA5/MVA1 (n = 5); vNY1 vs. vNY1/MVA1 (n = 5), and vNY5 vs. v-NY5/MVA1 (n = 5). Data are represented as mean ± SD. $^{**}p<0.01$; $^{***}p<0.001$; $^{****}p<0.0001$. (D). Immunoblot analyses of recombinant SARS-CoV-2 S protein using 1˚ and 2˚ sera (1:100) from immunized mice. A single representative serum is shown in each blot. (E). Neutralization assays of 2˚ sera collected from vaccinated mice using (i) Pseudovirus and (ii) SARS-CoV-2 virus infection: PBS/PBS control (n = 3); MVA5MVA1 (n = 5); vNY1/MVA1 (n = 5); and vNY5/MVA1 (n = 5). The dotted line represents assay limits of detection. $^{*}p<0.05$; $^{**}p<0.01$. (F). Quantification of anti-spike antibodies in mouse sera collected at 0.5 and 4.5 months after vaccination regimens using SF9 cells infected with WT-BAC or S-BAC. $^{*}p<0.05$; $^{**}p<0.01$; $^{****}p<0.0001$. (G). Pseudovirus neutralization assay using mouse sera collected at 0.5 months and 4.5 months after vaccination regimens: PBS/PBS control (n = 3); MVA5/MVA1 (n = 5); and vNY1/MVA1 (n = 5). ns–not significant. $^{*}p<0.05$. The dotted line represents assay limits of detection.

https://doi.org/10.1371/journal.pone.0257191.g002

3E), which revealed that all three regimens resulted in significantly increased numbers of $CD8^+$ Tem cells (Fig 3D), but not $CD4^+$ Tem cells (Fig 3E), in spleen tissue.

v-NY-S and MVA-S immunization generated neutralizing antibodies in immunized Syrian hamsters

C57BL/6 mice are not susceptible to SARS-CoV-2 infection, whereas Syrian hamsters serve as an appropriate animal model of respiratory infection by SARS-CoV-2 in human [54–65]. We subjected Syrian hamsters to the same prime-boost vaccination regimens, i.e., MVA5/MVA1, vNY1/MVA1 and vNY5/MVA1 (Fig 4A) as applied to mice (Fig 2A), except that we used a skin scarification inoculation approach for hamsters. A small scar formed at the immunization site, which healed within two weeks (S2A Fig), and the immunized hamsters remained healthy any did not exhibit weight loss (S2B Fig). Primary and secondary sera collected from these immunized hamsters specifically recognized SARS-CoV-2 S protein expressed on cell surfaces (Fig 4B). Quantification of all hamster sera by FACS demonstrated that boosting enhanced anti-spike antibody titers (Fig 4C), which was confirmed by immunoblotting (Fig 4D). Importantly, all three vaccination regimens generated anti-spike antibodies with high neutralization activity in both pseudotyped SARS-CoV-2 virus (Fig 4E, panel i) and live SARS-CoV-2 virus infection assays (Fig 4E, panel ii). Taken together, these data show that, as observed for mice, our vaccination regimens generated high antibody titers in hamsters that neutralized SARS-CoV-2 infection.

v-NY-S and MVA-S immunization reduce lung pathology in SARS-CoV-2-infected Syrian hamsters

Next, we performed challenge experiments in hamsters 2 weeks after vaccine boosting by intranasally (i.n) inoculating $1x10^5$ PFU/animal of SARS-CoV-2 virus into each hamster and then measuring changes in body weight till 3 d.p.i. (Fig 5A). Control hamsters (immunized with a PBS placebo) presented minor but detectable weight loss at 3 d.p.i., whereas those subjected to our vaccination regimens presented no obvious weight loss (Fig 5B). Previous studies showed that SARS-CoV-2 infection of Syrian hamsters results in virus replication in lung tissue and that virus titers often peaked from 2–4 d.p.i. and gradually cleared by 7 d.p.i. [54, 56, 58, 66–70]. Therefore, we sacrificed hamsters at 3 d.p.i. and then measured SARS-CoV-2 virus titers in their lungs (Fig 5C). None of the MVA5/MVA1- or vNY1/MVA1-vaccinated hamsters presented detectable levels of SARS-CoV-2 virus in their lung tissue, whereas virus titers of up to ~ $4x10^6$ $TCID_{50}$ were detected in the lungs of the placebo group (Fig 5C). Moreover, no virus was detected in nine vNY5/MVA1-immunized hamsters and only one such animal

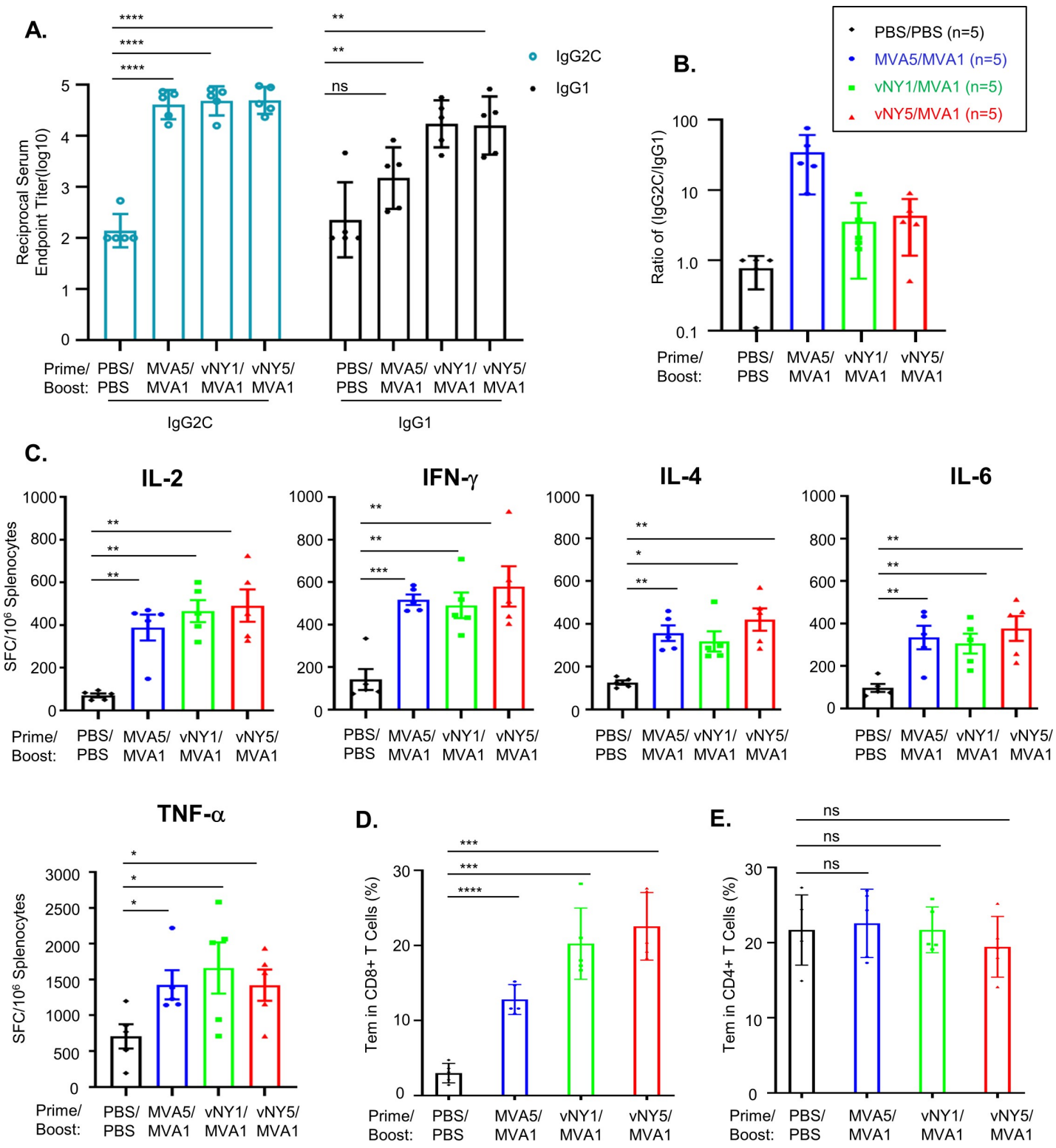

Fig 3. MVA5/MVA1, vNY1/MVA1 and vNY5/MVA1 vaccination regimens induce T_H1-biased immune responses. (A). End-point titers of SARS-CoV-2 spike-specific IgG2C and IgG1 antibodies in mouse sera collected 2 weeks after vaccination regimens. ns-not significant; $^{**}p<0.01$; $^{****}p<0.0001$. **(B).** End-point titer IgG2C/IgG1 ratio calculated based on data from **(A)** (n = 5 for each group). **(C).** ELISpot analyses of mouse splenocytes collected 4 weeks after vaccination regimens for their expression of IL-2, IFN-γ, TNF-α, IL4 and IL6 cytokines (n = 5 for each group). Data represented as mean ± SEM. SFC–spot-forming cells. $^{*}p<0.05$; $^{**}p<0.01$; $^{***}p<0.001$. **(D & E).** SARS-CoV-2 spike-specific $CD8^+$ (in D) and $CD4^+$ (in E) T effector memory cells ($CD44^+CD62L^-$) in splenocytes, as detected by flow cytometry (n = 5 for each group). Data represented as mean ± SD. ns–not significant; $^{***}p<0.001$; $^{****}p<0.0001$.

https://doi.org/10.1371/journal.pone.0257191.g003

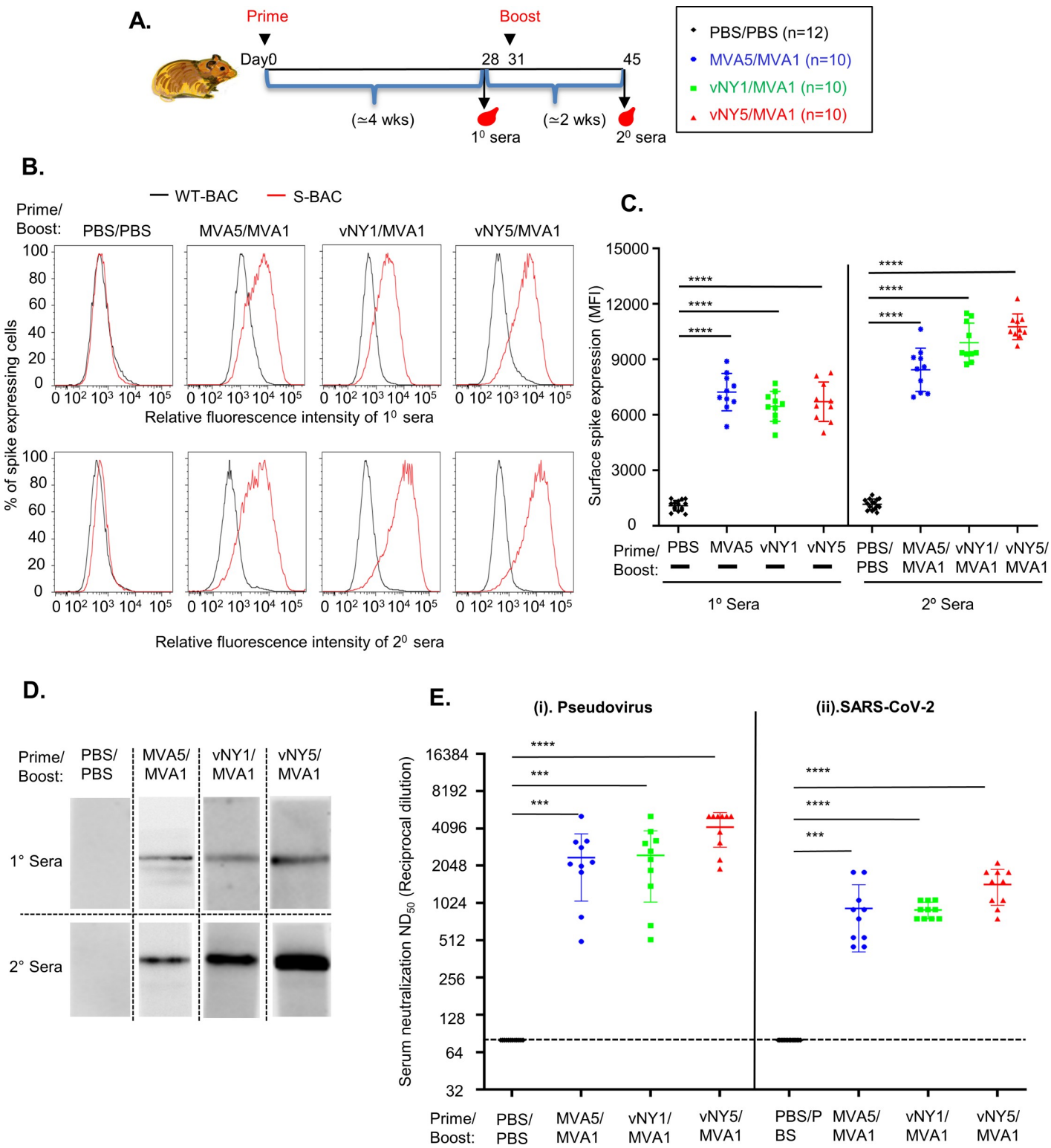

Fig 4. MVA5/MVA1, vNY1/MVA1 and vNY5/MVA1 prime-boost vaccination regimens generated SARS-CoV-2 spike-specific neutralizing antibodies in Syrian hamsters. (A). Timeline for hamster immunization and sera collection. **(B).** Primary and secondary sera from immunized hamsters recognized SARS-CoV-2 S protein on cell surfaces. Hamster sera collected 4 weeks after priming (1˚ sera) and 2 weeks after boosting (2˚ sera) were assessed for SARS-CoV-2-specific IgG antibodies by flow cytometry using SF9 cells infected with either S-BAC (red line) or WT-BAC (black line). A single representative serum is shown in each histogram. **(C).** Quantification of anti-spike antibody titers in 1˚ and 2˚ sera from hamsters in B, using the mean fluorescence intensity (MFI) value from FACS. Numbers of

hamsters for 1˚ and 2˚ sera collection are identical: PBS vs. PBS/PBS control (n = 15); MVA5 vs. MVA5/MVA1 (n = 10); vNY1 vs. vNY1/MVA1 (n = 10), and vNY5 vs. v-NY5/MVA1 (n = 10). Data are represented as mean ± SD. ****p<0.0001. **(D).** Immunoblots of 1˚ and 2˚ sera (1:20) from immunized hamsters using recombinant SARS-CoV-2 S protein. A single representative serum is shown in each blot. **(E).** Neutralization assays of 2˚ sera collected from vaccinated hamsters using (i) pseudovirus and (ii) SARS-CoV-2 virus infection: PBS control (n = 12); MVA5/MVA1 (n = 10); vNY1/MVA1 (n = 10); and vNY5/MVA1 (n = 10). The dotted line represents assay limits of detection. ***p<0.001; ****p<0.0001.

https://doi.org/10.1371/journal.pone.0257191.g004

presented residual amounts of virus (< 0.1% of the mean virus titer of the placebo group) (Fig 5C).

We further explored the impact of our MVA5/MVA1 regimen at 7 d.p.i. (Fig 5D). The weight loss of the placebo group was even more pronounced at 7 d.p.i. than at 3 d.p.i. (~10–15%), whereas that of MVA5/MVA1- immunized hamsters remained unchanged (Fig 5E). When we harvested lungs from immunized or placebo hamsters at 7 d.p.i. and measured SARS-CoV-2 virus titers and viral RNA levels, we found that no virus was detected in any of the hamsters (S3 Fig), but ~0^6 copies of viral RNA were detected in the lungs of the placebo group, whereas only ~10^2 copies were detected in MVA5/MVA1-immunized hamsters (Fig 5F).

To further validate our findings, we removed the lungs of experimental hamsters at 3 and 7 d.p.i. and processed them for histological examination (Fig 6). The lungs of placebo-infected hamsters at 3 d.p.i. presented diffuse congestion, shrinking of alveoli, hemorrhaging, and mononuclear cell infiltration (Fig 6A, open arrowheads). Moreover, bronchiolar epithelia vacuolization, necrosis and inflammatory exudates were also observed, and there was pronounced vasculitis and/or endothelialitis (Fig 6A, black arrows) involving both medium and small blood vessels disrupted by a mixture of immune infiltrates. Immunostaining with an antibody against SARS-CoV-2 nucleocapsid (NP) protein revealed some areas of peribronchiolar immunoreactivity (Fig 6A), mainly in the pneumocytes and less commonly in bronchiolar epithelial cells. Interestingly, despite the severe endothelial destruction observed by H&E staining, the SARS-CoV-2 NP antibody we deployed did not detect any positive viral-protein signal in the blood vessels of these placebo-infected hamsters. In contrast to the striking bronchointerstitial pneumonia observed in placebo-infected hamsters, there was only minimal to mild lung inflammation at 3 d.p.i. in the hamster groups subjected to the three vaccination regimens and SARS-CoV-2 NP protein signal was barely detectable (Fig 6B–6D).

We also examined the lung tissues of hamsters of the placebo and MVA5/MVA1 groups at 7 d.p.i. (Fig 6E & 6F). Profound type II pneumocyte hyperplasia (Fig 6E, open arrows) was observed for the placebo-infection group, accompanied by mild to moderate neutrophilic infiltrate and numerous megakaryocytes centered on an obliterated bronchiole. Immunohistochemistry revealed weak but positive anti-NP antibody signal in pneumocytes at the periphery of bronchiole-centered lesions of placebo-infected hamsters (Fig 6E). In contrast, the lungs of the MVA5/MVA1-infected group presented a less inflammatory phenotype at 7 d.p.i. and barely detectable anti-NP signal. Thus, taken together, our prime-boost vaccination regimens prevent SARS-CoV-2 viral spread in lung tissues and reduce inflammation and lung pathology.

Single immunization with v-NY-S partially protects Syrian hamsters from SARS-CoV-2 infection

We wished to establish if single-dose immunization with recombinant v-NY-S virus could provide protection against SARS-CoV-2 in Syrian hamsters. Hamsters were immunized with PBS (placebo), 1x10^7 or 5x10^7 PFU/animal of v-NY-S by skin scarification and then sera were collected 2 weeks later (Fig 7A). The sera were subjected to a SARS-CoV-2 pseudovirus neutralization assay, which showed that priming with v-NY-S alone generated neutralizing antibodies

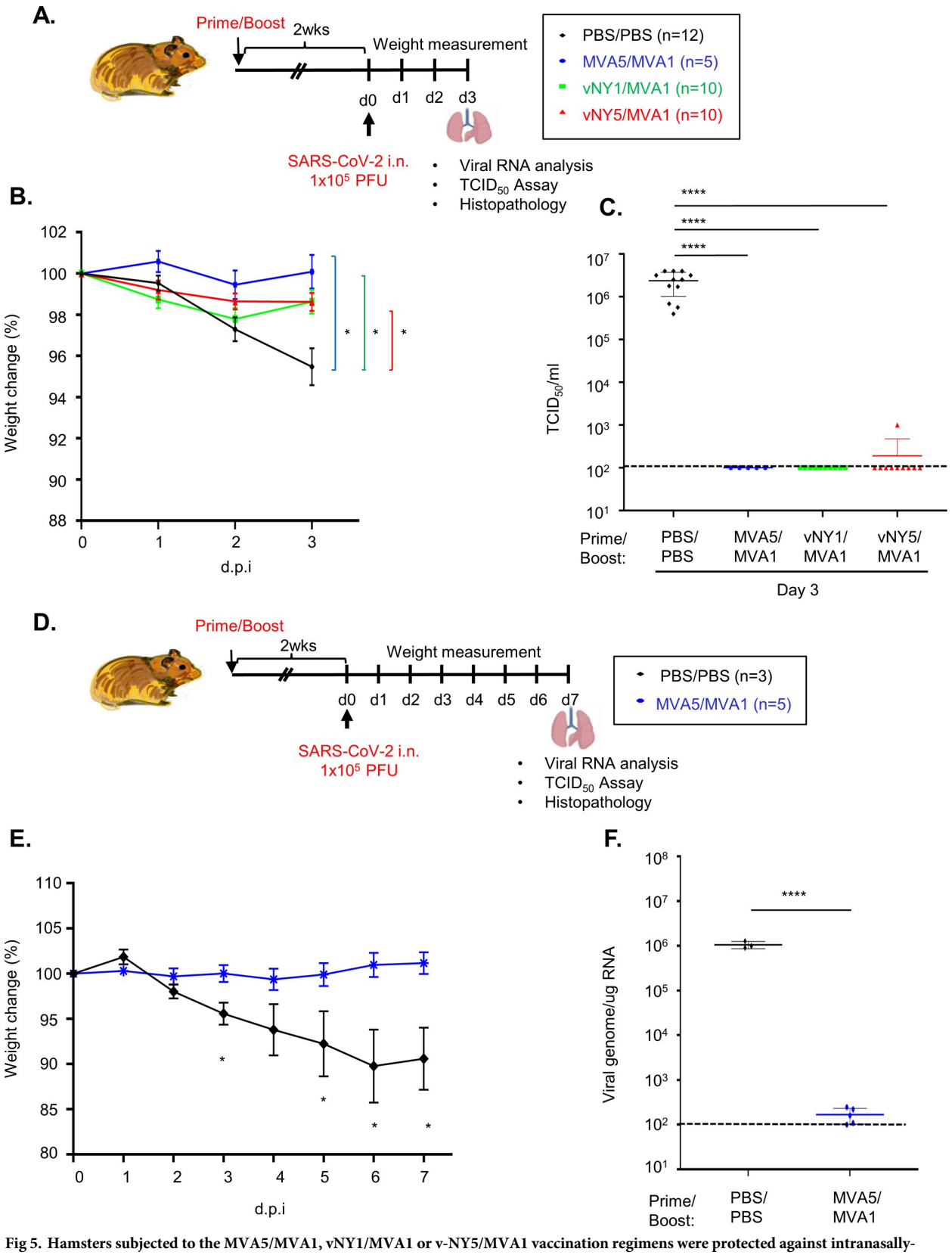

Fig 5. Hamsters subjected to the MVA5/MVA1, vNY1/MVA1 or v-NY5/MVA1 vaccination regimens were protected against intranasally-administered SARS-CoV-2 infection. (A). Timeline of the immunization and challenge experiments. Hamsters immunized with one of three prime-boost vaccination regimens (MVA5/MVA1, vNY1/MVA1 or vNY5/MVA1), or placebo (PBS) as a control, were challenged i.n. with $1x10^5$ PFU SARS-CoV-2 virus, before harvesting lungs at 3d.p.i.. **(B).** Weight change of hamsters within 3 days of SARS-CoV-2 challenge. Data represented as mean ± SEM. $^*p<0.05$. **(C).** $TCID_{50}$ value of SARS-CoV-2 in lung tissue of hamsters at 3 d.p.i. after SARS-CoV-2 challenge: PBS/

PBS control (n = 12); MVA5/MVA1 (n = 5); vNY1/MVA1 (n = 10); and vNY5/MVA1 (n = 10). Data represented as mean ± SD. ****p<0.0001. **(D).** Timeline of the immunization and challenge experiments. Hamsters immunized with one prime-boost vaccination regimen (MVA5/MVA1), or placebo (PBS/PBS) as a control, were challenged i.n. with $1x10^5$ PFU SARS-CoV-2 virus, before harvesting lungs at 7d.p.i.. **(E)** Weight change of hamsters within 7 days of SARS-CoV-2 challenge: PBS/PBS control (n = 3); and MVA5/MVA1 (n = 5). Data represented as mean ± SEM. *p<0.05. **(F).** SARS-CoV-2 genomic RNA in lungs of MVA5/MVA1-immunized hamsters at 7 d.p.i. after SARS-CoV-2 challenge: PBS/PBS control (n = 3); and MVA5/MVA1 (n = 5). Unless stated otherwise, data are represented as mean ± SD. The dotted line represents assay limits of detection. ****p<0.0001.

https://doi.org/10.1371/journal.pone.0257191.g005

against SARS-CoV-2 virus in a dosage-dependent manner (Fig 7B). Then we performed challenge experiments and monitored SARS-CoV-2 virus titers in lungs at 3 d.p.i. (Fig 7C). Virus titers were ~10^6 PFU/animal in the placebo-infected group, but virus titers were >100-fold lower in hamsters subjected to single immunization with v-NY-S at either dosage ($1x10^7$ or $5x10^7$ PFU/animal), showing that single immunization had already provided partial protection against SARS-CoV-2 infection. Upon removing lungs for histological examination, we observed that the placebo-infected group presented a severe pathological phenotype including diffuse congestion, shrinking of alveoli, hemorrhaging, and mononuclear cell infiltration (Fig 7D, open arrowheads). Moreover, immunostaining for SARS-CoV-2 NP protein also revealed widespread peribronchiolar immunoreactivity (Fig 7D, arrowheads) in the lungs of the placebo group. In contrast, the lung pathology of the vNY1-infected (Fig 7E) and vNY5-infected (Fig 7F) groups was much milder than observed for the placebo-infected group, displaying lower immune cell infiltration, rare epithelial degeneration and an absence of vasculitis/endothelialitis. Viral NP immune signal in lung tissues was also significantly lower in the vNY1 and vNY5 groups relative to the placebo group (rightmost panels in Fig 7E & 7F).

Sera from vaccinated mice partially cross-neutralize SARS-CoV-2 variants of concern

Recently, circulation of new SARS-CoV-2 variants of concern (VOC) has become prevalent, entailing a risk of increasing resistance to the neutralizing antibodies generated by SARS-CoV-2 vaccines. Accordingly, we used pseudotyped SARS-CoV-2 virus neutralization assays to test sera from our prime-boost vaccinated mice for their ability to cross-neutralize SARS-CoV-2 variants (Fig 8). Although statistical analyses did not reveal a significant neutralization difference among the three immunization regimens to each variant, the mean neutralization titers of the α and γ variants were similar to that of the wild type whereas the mean titers of β, B.1.617 and δ variants appeared much lower than the wild type (Fig 8A). For sera generated according to each regimen (Fig 8B–8D), we divided the value of ND_{50} for wild type by that of each variant to obtain the fold decrease in neutralization for each variant relative to wild type (Fig 8B–8D). We noticed that vNY5/MVA1 regimen maintained the least decrease of neutralization towards all variants (Fig 8D) followed by vNY1/MVA1(Fig 8C) and MVA5/MVA1 (Fig 8B). Overall, antibodies from mice vaccinated with the heterologous prime-boost regimens, vNY1/MVA1 and vNY5/MVA1, appeared to display better cross-neutralization against different variants than those with the homologous prime-boost regimen (MVA5/MVA1).

A heterologous prime-boost immunization regimen with v-NY-S generates higher titers of neutralizing antibodies than a homologous prime-boost regimen

Our current regimens comprise both homologous (MVA5/MVA1) and heterologous (vNY1/MVA1 and vNY5/MVA1) prime-boost combinations, with these latter generating strong and long-lasting neutralizing antibody responses (Fig 2F). We wanted to explore other prime-

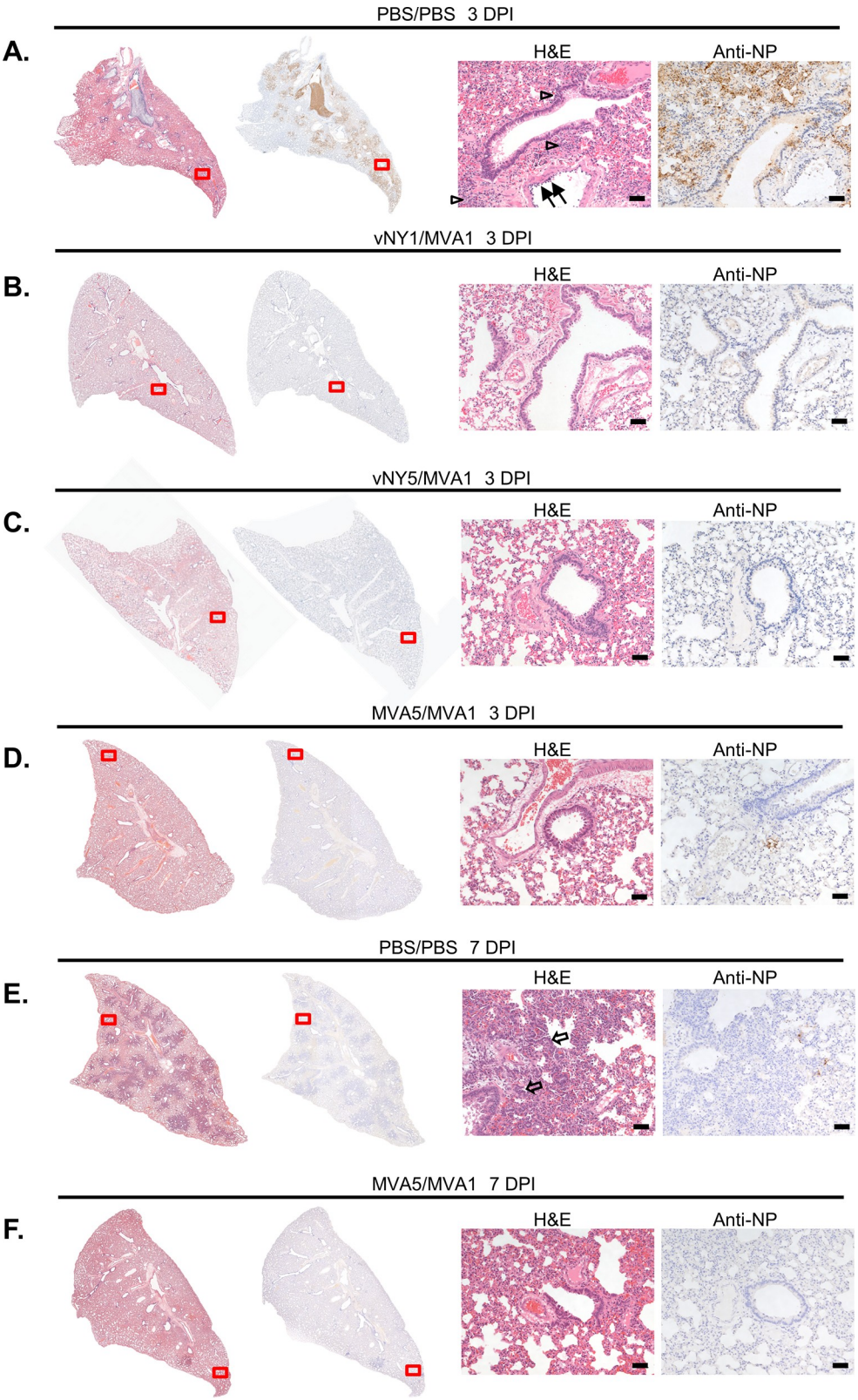

Fig 6. Lung pathology and immunohistochemistry of hamsters after SARS-CoV-2 challenge. (A). H&E and immunohistochemical staining of lungs of the placebo (PBS/PBS) infection hamster group at 3 d.p.i.. H&E staining showed severe bronchointerstitial pneumonia with the alveolar walls thickened by edema, capillary congestion and

variable immune cell infiltration (open arrowheads). The vascular endothelia were frequently disrupted by immune infiltrates (vasculitis/endotheliolitis, black arrows). Immunohistochemistry of SARS-CoV-2 NP protein revealed prominent peribronchiolar staining (arrow heads). **(B, C & D).** H&E and immunohistochemical staining of lungs from the vNY1/MVA1 (B), vNY5/MVA1 (C) and MVA5/MVA1 (D) hamster groups at 3 d.p.i.. Compared to the placebo (PBS/PBS) infection hamster group, lung architecture was better preserved, there was much less immune cell infiltration, and SARS-CoV-2 NP staining signal was barely detectable. **(E).** H&E and immunohistochemical staining of lungs of the placebo (PBS/PBS) infection hamster group at 7 d.p.i.. H&E staining revealed prominent type II pneumocytic hyperplasia (open arrows) with variable immune cell infiltration. Immunohistochemistry of SARS-CoV-2 NP protein detected dispersed positive signals at the edges of regenerative foci. **(F).** MVA5MVA1-immunized hamsters displayed minimal lung pathology and scant SARS-CoV NP immunolabeling at 7 d.p.i.. The enlarged views of H&E and immunohistochemistry-stained regions are marked by red boxes. The scale bar represents 50 μm.

https://doi.org/10.1371/journal.pone.0257191.g006

boost combinations involving v-NY-S as an alternative strategy to improve immune responses. As shown in Fig 9A, unlike MVA5/MVA1 (Fig 2C), prime-boosting with a homologous vNY1/vNY1 strategy did not increase anti-spike antibody titers after boosting (Fig 9A). We rationalize that homologous prime-boosting with a replicating virus such as v-NY-S is not a good immunization strategy. Interestingly, heterologous priming with v-NY-S at $1x10^7$ PFU, followed by a boost with 5 μg recombinant spike protein (rS) plus adjuvant, enhanced anti-spike antibody titers (Fig 9A) and neutralizing activity (Fig 9B). In addition, we compared the route of priming between skin scarification (vNY1/MVA1) and intranasal inoculation (vNY0.1/MVA1) for v-NY-S and found that the latter route generated higher anti-spike antibody levels (Fig 9A) and neutralizing activity (Fig 9B) with only 1/10 of virus inoculum. These data are very encouraging and will aid in future vaccination strategies. Discussions are ongoing as to whether heterologous prime-boosting of COVID vaccines elicits more potent immune responses than a homologous prime-boost strategy [71–73]. We argue that mix-and-match vaccination strategies are an important consideration for designing the next generation of SARS-CoV-2 vaccines.

Discussion

In this study, we have demonstrated in preclinical models the safety and immunogenicity of recombinant vaccinia viruses expressing SARS-CoV-2 virus spike protein. All three of the prime-boost vaccination regimens with v-NY-S and MVA-S recombinant viruses elicited strong and long-lasting neutralizing antibody responses against SARS-CoV-2, and also generated a T_H1-biased T cell response that can promote pathogen clearance. Importantly, we have demonstrated that our vaccination regimens protected Syrian hamsters (representing an appropriate animal model of SARS-CoV-2-induced respiratory disease in human) from weight loss, elicited rapid clearance of SARS-CoV-2 virus, and reduced immune infiltrates in lung tissue. Previous studies have revealed that virus shedding is often associated with a high viral titer in lung tissues [42, 54, 68]. Bricker et al. (2021) showed that virus titers in vaccinated hamsters were cleared by day 3, and no virus shedding was detected in nasal swabs even as early as day 2 [68]. Furthermore, Liu et al. (2021) found that vaccinated transgenic mice did not shed virus as early as day 2 when virus was cleared from the lungs [42]. Since virus was cleared from the lung tissue of our prime-boost vaccinated animals, it is likely that virus shedding in these animals is limited.

When we compared data from male versus female hamsters in terms of weight loss and virus replication in lungs, we did not observe noticeable sex-associated differences in these hamsters after challenge with SARS-CoV-2 virus. Interestingly, Dhakal et al. (2021) reported that hamsters of both sexes exhibited similar weight loss, virus titers in lungs and cytokine response in the first 5–7 days after SAS-CoV-2 challenge [74]. However, they also showed that, starting from day 7 up to 4 weeks, female hamsters developed greater antibody responses and

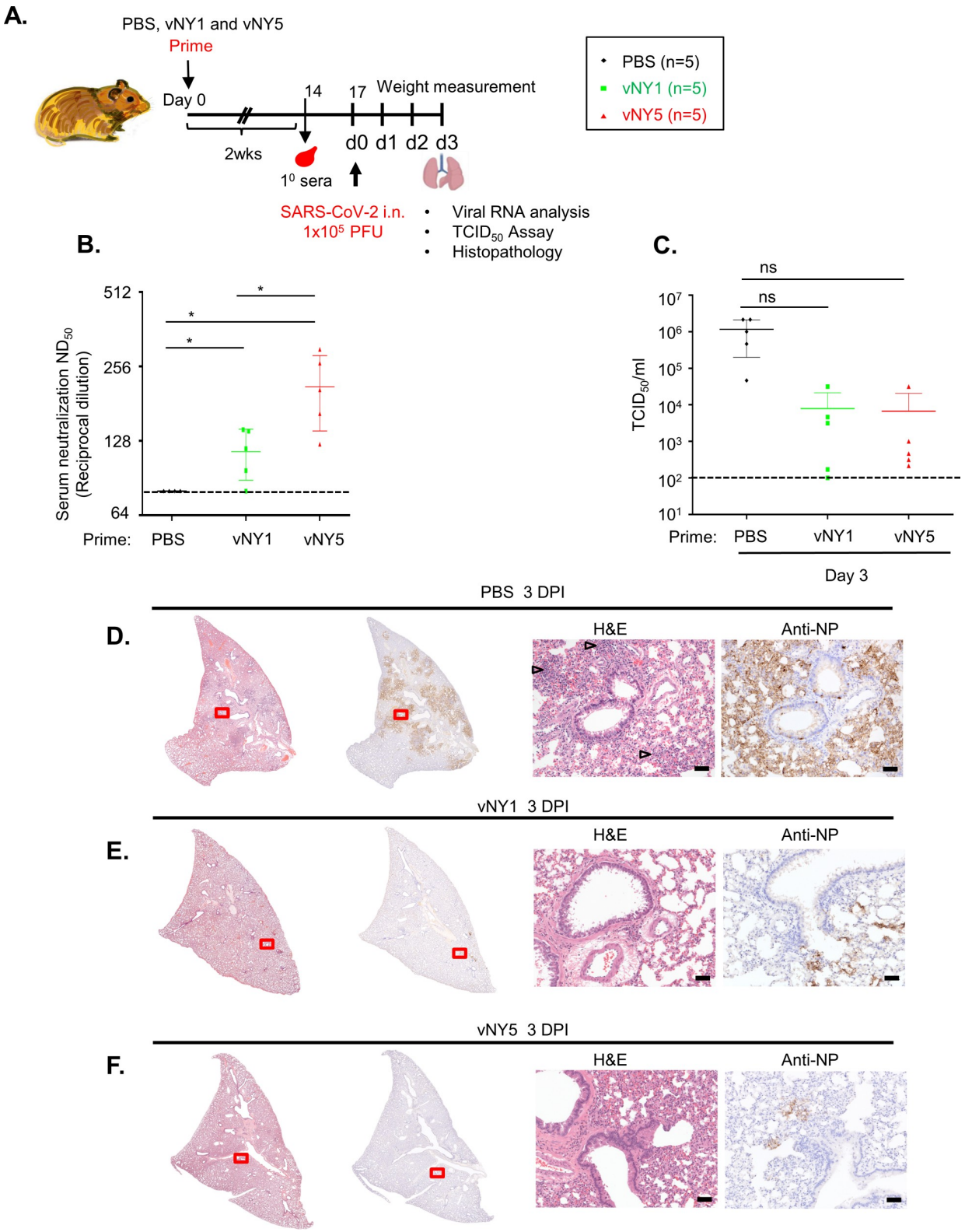

Fig 7. Single-dose vNY1 or vNY5 vaccination partially protected hamsters from intranasally-administered SARS-CoV-2 infection. (A). Timeline showing the immunization and challenge experiment. Hamsters immunized with a single dose of vNY1, vNY5 or placebo (PBS) were challenged i.n. with $1x10^5$ PFU SARS-CoV-2 virus and then lungs were harvested at 3 d.p.i.. **(B).** Pseudovirus neutralization assays of the 1˚ sera collected 2 weeks after vaccine priming in hamsters. PBS control (n = 4); vNY1 (n = 5); and vNY5 (n = 5). Data represented as mean ± SD. The

dotted line represents assay limits of detection. *p<0.05. **(C).** $TCID_{50}$ values for lungs from hamsters of the placebo (PBS), vNY1 and vNY5 groups at 3 d.p.i. after SARS-CoV-2 challenge (n = 5 for each group). Data represented as mean ± SD. The dotted line represents assay limits of detection. ns- not significant. **(D).** H&E and immunohistochemical staining of lungs of the placebo (PBS) infection hamster group at 3 d.p.i.. H&E staining revealed an identical pathology to that shown in Fig 6A, revealing severe bronchointerstitial pneumonia with the alveolar walls thickened by edema, capillary congestion and variable immune cell infiltration (open arrowheads). Immunohistochemistry of SARS-CoV-2 NP protein revealed prominent peribronchiolar staining (arrowheads), with the vascular endothelia frequently being disrupted by immune infiltrates. **(E and F).** H&E and immunohistochemical staining of hamster lungs primed with vNY1 (in E) or vNY5 (in F) at 3 d.p.i.. The lung architecture was largely preserved, displaying reduced immune cell infiltration relative to the placebo infection group and SARS-CoV-2 NP protein was barely detectable by immunohistochemistry. The scale bar represents 50 μm.

https://doi.org/10.1371/journal.pone.0257191.g007

recovered from weight loss faster than male hamsters [74]. Because all our experiments were terminated within 1 week after SARS-CoV-2 challenge it could explain a lack of sex-associated difference in our experiments.

Hamster is a good animal model of SARS-CoV-2 with several advantages. It is suitable to study virus replication and transmission by contact and aerosols [54, 75]. Most of hamsters infected with SARS-CoV-2 do not die, which is consistent with human infections, and the pathological features of the lungs in the infected animals resemble those observed in COVID-19 patients [56, 76, 77]. Hamster is relatively low cost when compared with other animal models, such as ferrets [78] and non-human primates [79], and has been shown to mount an effective antibody response that clears virus within one week, making it a suitable model to study vaccine efficacy and antiviral drugs [54, 56, 80]. On the other hand, several limitations of the hamster model exist. SARS-CoV-2 infection in humans affects multiple organ systems including the heart, kidneys, liver, spleen and large intestine [81, 82] whereas in hamsters live virus mainly replicates in respiratory tracts with little evidence of infectious virus in other organs, despite the detection of viral RNA in non-respiratory tissues [55, 83]. Furthermore, a lack of hamster-specific biological reagents makes it difficult to characterize immune responses and the mechanisms of pathogenesis in hamsters.

A successful vaccine against SARS-CoV-2 should stimulate both humoral and cellular immune responses to inhibit virus replication and prevent disease in the host [84]. In both mouse and hamster model our prime-boost immunization with MVA-S and v-NY-S generated high titers of neutralizing antibodies. Evidence from preclinical studies in nonhuman primates and hamsters indicted that vaccine-induced SARS-CoV-2 neutralizing antibodies correlate with protection against lung infection and clinical disease [19, 55, 85]. While it is difficult to study T-cell immune response in hamsters, our immunization regiments induced T_H1-biased immune response and effector memory $CD8^+$T cells in mice, consistent with other studies using MVA-based SARS-CoV-2 vaccines [41–43, 86]. Interestingly, Tan, et al (2021) reported that early induction of interferon-γ secreting SARS-CoV-2 specific T cells correlates with mild disease and rapid virus clearance, implying an important role of T cell immunity in host protection [87]. How to improve a SARS-CoV-2 vaccine to induce a coordinated B and T responses will be of great importance in the future.

SARS-CoV-2 vaccines developed by Moderna, Pfizer/BioNTech, Novavax and Janssen Pharmaceutical companies expressed a designed SARS-CoV-2 spike protein, S-2P, which contain two proline substitutions at K986 and V987 to stabilize the prefusion conformation of spike protein [19, 85, 88, 89]. It is thought the S-2P design could improve protein stability and elicit high titers of neutralizing antibodies [19, 85, 88, 89]. We did not modify the spike protein in our recombinant virus constructs primarily because of two reasons: (i) Vaccinia viral promoters are known to be much stronger than cellular promoters [90, 91] so the spike protein abundance and stability may not be a concern. (ii). We think that the natural spike protein conformation may provide a large repertoire of antigenic epitopes to generate neutralizing antibodies against SARS-CoV-2 virus. Our neutralizing antibodies induced strong neutralizing

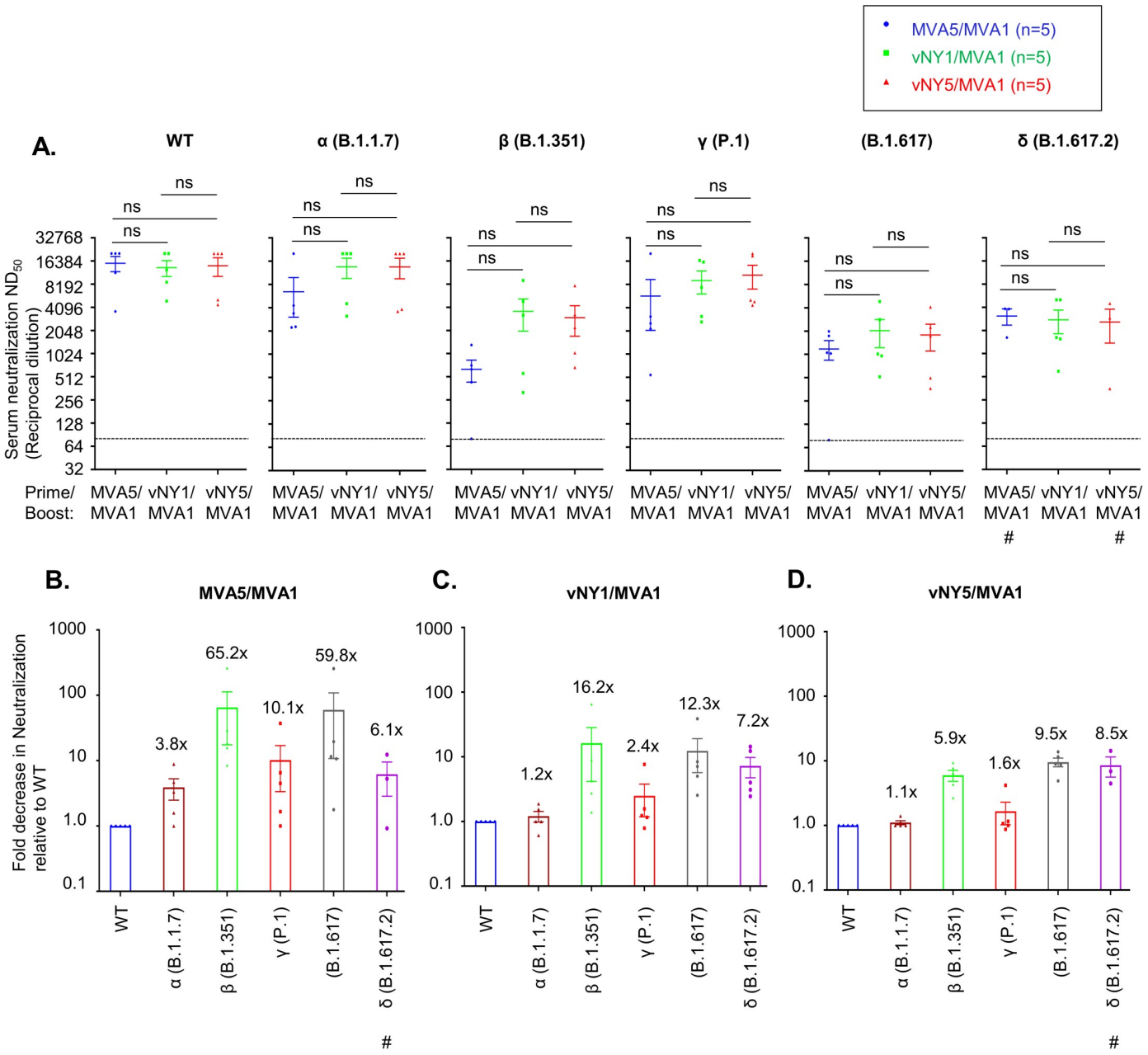

Fig 8. Sera from vaccinated mice partially cross-neutralized SARS-CoV-2 variants of concern. (A). Neutralization assays of secondary sera collected from vaccinated mice (regimens MVA5/MVA1, vNY1/MVA1 and vNY5/MVA1) following SARS-CoV-2 pseudotyped virus with spike protein from WT and variants α (B.1.17), β (B.1.351), γ (P.1), B1.617 and δ (B.1.617.2). The dotted line represents assay limit of detection. # represents n = 3. ns-not significant. **(B-D).** Fold decrease for immunized sera from MVA5/MVA1 (B), vNY1/MVA1(C) and vNY5/MVA1(D) vaccination regimens in neutralization assays of individual variants relative to WT pseudovirus. Fold change was calculated by dividing the ND_{50} titer of each immunized serum against WT pseudovirus with the ND_{50} titer of the same serum against variant pseudovirus. # represents n = 3. The dotted line represents assay limit of detection. Data are represented as mean ± SEM.

https://doi.org/10.1371/journal.pone.0257191.g008

titers, supporting that rationale. Besides, Tscherne et al (2021) constructed a vaccinia MVA-SARS-2-S vaccine that expresses a native SARS-CoV-2 spike protein and their results also showed high neutralizing antibodies were induced [86]. Moreover, the AstraZeneca vaccine, which lacks pre-fusion 2P stabilization, provided sufficient protection during clinical trials [92, 93]. It is intriguing that a new version of spike modification known as HexaPro, that contains

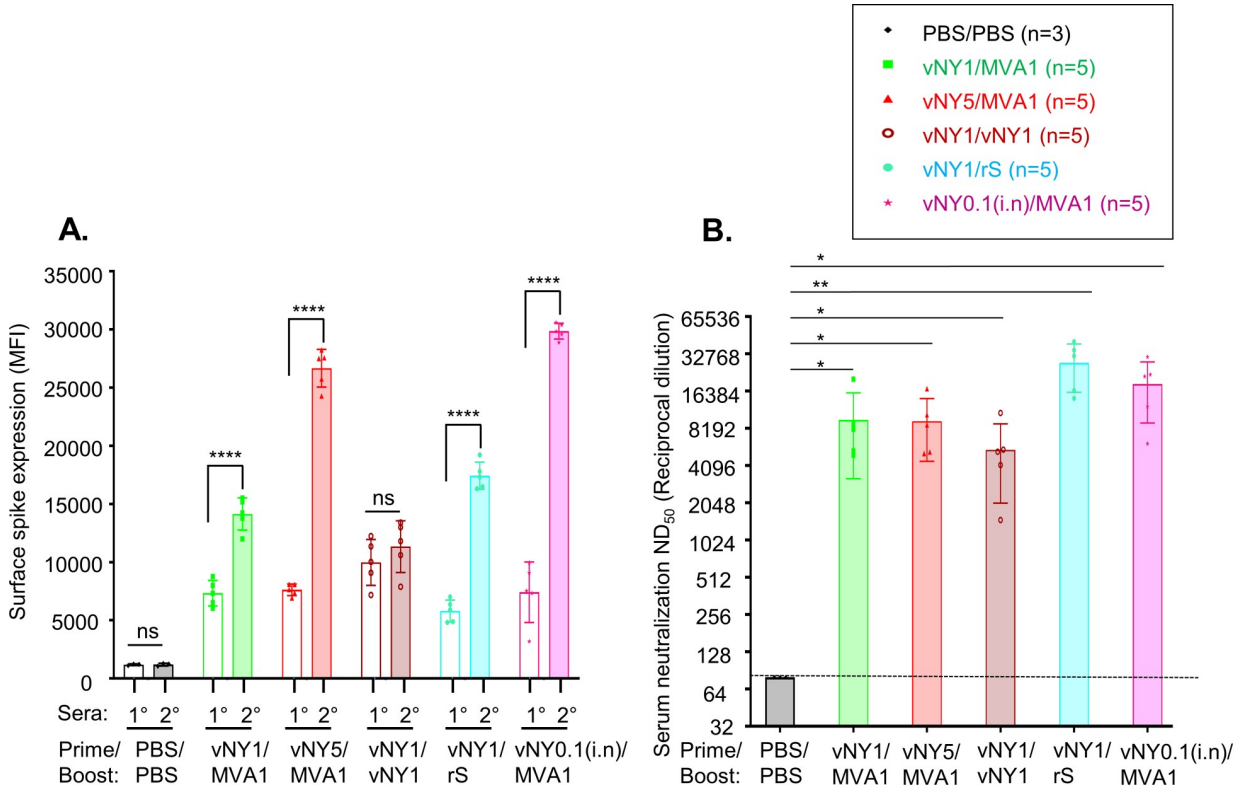

Fig 9. Heterologous prime-boost and intranasal inoculation with v-NY-S enhances production of SARS-CoV-2 spike-specific neutralizing antibodies. (A). Quantification of anti-spike antibody titers in primary (1˚, transparent bars) and secondary (2˚, filled bars) sera from mice by staining cell surface spike protein on insect cells using FACS, as shown by the mean fluorescence intensity (MFI). Sera were collected from identical mice after prime (1˚) and boost (2˚). Numbers of mice in each prime-boost groups are shown on top of the figure. Data are represented as mean ± SD. $^{****}p<0.0001$; ns-not significant. **(B).** SARS-CoV-2 pseudotyped virus neutralization assays for 2˚ sera collected from mice after different prime-boost regimens. The dotted line represents assay limit of detection. rS: recombinant spike protein. $^{*}p<0.05$; $^{**}p<0.01$.

https://doi.org/10.1371/journal.pone.0257191.g009

six proline substitutions to further stabilize the pre-fusion S protein, was reported [94]. Whether HexaPro represents a promising antigen for vaccine design will be interesting to know in the future.

While we were testing our vaccination regimens, several research groups published studies showing that MVA-based vaccines provided protection against SARS-CoV-2 infection in hACE2 transgenic mice [41, 86, 95] and macaques [43]. The results of our recombinant MVA-S-based vaccines are consistent with those findings. Our study further explores the utility of the replication-competent v-NY strain, revealing that it could prove just as promising as the MVA strain in tackling SARS-CoV-2. The MVA strain that is growth-restricted in mammalian cells has been widely used in vaccine clinical studies due to its safety features. In contrast, v-NY was originally isolated and developed as a replicating vaccinia vector [96]. A plaque-purified New York City Board of Health strain of vaccinia virus was established from a commercial preparation of smallpox vaccine (Dryvax) via three successive rounds of plaque-purification in BSC-40 cells. A master seed stock of this virus was prepared in human diploid MRC-5 cells, which was then used as the parental virus (v-NY) to construct a recombinant virus expressing the envelope glycoproteins of HIV-1 (HIVAC-1e) later used for FDA-approved clinical trials [44]. Since then, master seed stocks of v-NY have been extensively characterized in terms of sterility, mycoplasma, adventitious viruses, plaque morphology, neutralization by vaccinia-specific monoclonal and polyclonal antisera, neurovirulence and

genome restriction analysis [44]. Unlike NYVAC [97], which is a highly attenuated virus constructed from the Copenhagen strain of vaccinia virus by specific genetic deletions, v-NY is a replication-competent virus and has not gone through any "attenuation protocol", such as the repeated passages for MVA. The *in vitro* and *in vivo* characteristics of v-NY are similar to its parent virus, the New York City Board of Health strain of smallpox vaccine [44–47]. It is well known that insertion of a foreign gene into the *tk* locus of vaccinia viral genome such as v-NY will result in further attenuation of vaccinia virus virulence in mice [31]. In terms of safety profile, the recombinant v-NY virus (HIVAC-1e) has been tested in Phase I and II studies [46, 47]. Moreover, v-NY has been used as a control virus in many animal studies and, in all cases, the elicited responses appear very similar to how smallpox vaccines behave in humans [44, 45, 98, 99].

There are several reasons why we elected to conduct v-NY-S inoculation via skin scarification. First, Langerin^{+} dermal dendritic cells have been shown to effectively present antigen upon skin scarification with vaccinia virus [100]. Secondly, more antibodies are generated upon scarification than via intramuscular inoculation [101]. Thirdly, given experience with the global smallpox vaccination program, skin scarification by means of a bifurcated needle to prick the skin 15 times within a few seconds is a convenient and efficient way to inoculate a large human population during a pandemic. It is possible that for people displaying acute skin breaks such as acne or suffering chronic skin conditions such as eczema or atopic dermatitis, the side-effects may be more serious and should be taken into consideration. In addition, the inoculation site on the arm should be properly cared for so that the virus does not spread. Overall, the availability of both recombinant MVA and v-NY viruses expressing SARS-CoV-2 S protein allows studies to determine whether genetic properties of the viral vector may modulate immune responses leading to differential vaccine efficacies. To this end, it may be worth thinking that a better "placebo vaccine" control than PBS alone would be supernatants of cells that do not express the spike construct but that are prepared the same way as the vaccine. These preparations would contain a secretome including extracellular vesicles and other xenogeneic materials that might contribute to responses like cytokines, albeit presumably non-specific. It will be useful to include such controls in the future experiments.

Most SARS-CoV-2 vaccines currently on the market require a two-dose prime-boost vaccination program to generate sufficient protective immunity [12, 18, 20, 23, 102–107]. Several Adenovirus-based vaccines (such as ChAdOx) were demonstrated as quite effective following two dosages [19, 20, 55, 108–110], though single immunization is sufficient for the Ad26.COV2.S vaccine [19]. Because the fast rise of SARS-CoV-2 variants whether these vaccines can adequately control the COVID pandemic remains unclear. As the stability of currently available COVID vaccines depends on different temperatures of the "cold chain" for storage and transportation, reliance on these vaccines alone for global vaccination may be difficult. In this context, the stability of the lyophilized smallpox vaccine, from which the v-NY vector was derived, may present certain advantages. Thus, these findings from deployment of our recombinant v-NY-S and MVA-S vaccine candidates in a prime-boost vaccination regimen may represent a very useful approach to tackling SARS-CoV-2 infections globally.

Materials and methods

Animals and ethics statement

Eight-week-old female C57BL/6 mice (Charles River strain) were purchased from BioLASCO Taiwan Co. Ltd. Eight-week-old male and female Syrian hamsters (*Mesocricetus auratus*) were purchased from the National Laboratory Animal Center, Taiwan. All animal protocols were approved by the Institutional Animal Care and Utilization Committee of Academia Sinica and

Table 1. Reagent list.

Reagent name	Company	Catalogue no.
SARS-CoV-2 (2019-nCoV) Spike RBD antibody	Sino Biological	40592-T62
SARS-CoV/SARS-CoV-2 (COVID-19) spike antibody [1A9]	GeneTex	GTX632604
SARS-CoV/SARS-CoV-2 (COVID-19) Nucleocapsid antibody, Rabbit Mab	Sino Biological	40143-R001
Anti-Rabbit IgG (whole molecule), F(ab')2 fragment—FITC antibody	Sigma	F1262
Goat anti-Mouse IgG (H+L) Secondary antibody, HRP	ThermoFisher Scientific	31430
Goat anti-Mouse IgG (H+L) Secondary antibody, HRP	Invitrogen	PA1-28823
Cy5 Affinipure Goat anti-Mouse IgG (H+L)	Jackson Immuno Research	115-175-146
Goat anti-Syrian Hamster IgG Secondary antibody, FITC	eBioscience	11-4211-85
Goat anti-Mouse IgG2c Secondary antibody, HRP	Invitrogen	PA1-29288
Goat anti-Mouse IgG1 Secondary antibody, HRP	Invitrogen	PA1-74421
PE/Cyanine7 anti-Mouse CD3 Antibody	BioLegend	100220
FITC-anti-Mouse CD4 Antibody	BioLegend	100510
Pacific Blue- anti-Mouse CD8 Antibody	BioLegend	100725
PE anti-Mouse/Human CD44 Antibody	BioLegend	103008
APC anti-Mouse CD62L Antibody	BioLegend	104412
DAPI, Fluropure, grade	Invitrogen	D21490
VECTASHIELD, Antifade Mounting Medium	Vector Laboratories	H-1000
PepTivator SARS-CoV-2 Prot_S	Miltenyi Biotec	130-126-700
Mouse IFN-γ ELISpot PLUS Kit (ALP), strips	MABTech	3321-4AST-2
Mouse IL-2 ELISpot PLUS Kit (ALP)	MABTech	3441-4APW-2
Mouse IL-4 ELISpot PLUS Kit (ALP)	MABTech	3311-4APW-2
Mouse IL-4 ELISpot PLUS Kit (ALP)	MABTech	3361-4APW-2
Mouse TNF-α ELISpot PLUS Kit (ALP)	MABTech	3511-4APW-2
Dako EnVision+ System–HRP-labeled polymer	Dako	K4001
Alhydrogel (2%)	InvivoGen	Vac-alu-250

https://doi.org/10.1371/journal.pone.0257191.t001

were conducted in strict accordance with the guidelines on animal use and care of the Taiwan National Research Council's Guide. Immunization and blood collection from animals were performed under isoflurane anesthesia. Animals were sacrificed with carbon dioxide at the end-point of the experiment and all precautions were taken to minimize the suffering to the animals throughout the study.

Cells, viruses, and reagents

BSC40 cells were cultured in DMEM supplemented with 10% fetal bovine serum (FBS) (Gibco) and 1% penicillin-streptomycin (PS) (Gibco). BHK21 cells were cultured in RPMI medium supplemented with 10% FBS and 1% PS. HuTK-143 cells were cultured in MEM medium supplemented with 10% FBS and 1% PS. The v-NY strain of vaccinia virus was grown on BSC40 or HuTK-143 cells as described previously [96, 98, 111–114]. The MVA strain of vaccinia virus (VR-1508, ATCC) was grown on BHK21 cells. SARS-CoV-2 TCDC#4 (hCoV-19/Taiwan/4/2020) is a local isolate and it was propagated on Vero-E6 cells. All antibodies and reagents are listed in Table 1 below.

Construction of recombinant vaccinia viruses

To generate recombinant vaccinia viruses expressing SARS-CoV-2 S protein (Isolate Wuhan-Hu-1, NC_045512), a human codon-optimized open reading frame (ORF) encoding full-length SARS-CoV-2 S protein was inserted into a pSC11 plasmid and under regulatory control

by an early and late p7.5k promoter to obtain pSC11-S plasmid [115]. The pSC11-S plasmid was transfected into HuTK-143 cells infected with the wild type v-NY virus strain. Lysates were then harvested for multiple rounds of plaque purification of the recombinant virus, named v-NY-S, on HuTK-143 in the presence of 25 μg/ml 5-Bromo-2′-Deoxyuridine (BrdU), as described previously [113]. The recombinant MVA strain expressing SARS-CoV-2 S protein, MVA-S, was generated as described for v-NY-S except that BHK21 cells were used and plaque purification was performed in the presence of X-gal (150 μg/ml). Both MVA-S and v-NY-S were subsequently amplified in roller bottles, and the virus stocks were partially purified using a 36% sucrose gradient and titrated prior to use, as described previously [116].

Immunofluorescence staining of cell surface S protein

BHK21 and BSC40 cells were infected respectively with MVA-S or v-NY-S at a multiplicity of infection (MOI) of 5 PFU/cell for 1 h, washed with PBS, and then incubated in growth media for a further 12 h. The cells were then washed with PBS and fixed with 4% paraformaldehyde, before being immunostained with SARS-CoV-2 anti-RBD antibody (40592-T62) at a dilution of 1:500 for 1 h at room temperature. Then, the cells were washed with PBS and stained for the secondary antibody FITC-conjugated goat anti-Rabbit IgG Ab (F1262, 1:500 dilution) for 1 h at room temperature, followed by staining with DAPI (5 μg/ml, D21490, Molecular Probes) for 5 min and mounting with Vectashield mounting solution (H-1000, Vector Laboratories). Images were taken using a Zeiss LSM 710 confocal microscope with a 63x objective lens, as described previously [117].

Prime-boost immunization regimens in mice

Eight-week-old female C57BL/6 mice were housed in the Animal Facility of Academia Sinica (Taipei, Taiwan) for at least 3 days prior to vaccination experiments. We primarily used three regimens of two-dosage prime/boost immunization (depicted in Fig 2A): (1) MVA5/MVA1—intramuscular (i.m.) inoculation of MVA-S in the right hind limb at $5x10^7$ PFU/animal, followed by an i.m. boost 4 weeks later of $1x10^7$ PFU/animal of MVA-S virus; (2) vNY1/MVA1—tail scarification (t.s) of v-NY-S at $1x10^7$ PFU/animal, followed by an i.m. boost 4 weeks later of $1x10^7$ PFU/animal of MVA-S virus into the right hind limb; and (3) vNY5/MVA1- t.s. of v-NY-S at $5x10^7$ PFU/animal, followed by an i.m. boost 4 weeks later of $1x10^7$ PFU/animal of MVA-S virus into right hind limb. Additional prime/boost combinations were designed in order to obtain mouse sera for pseudotyped SARS-CoV-2 virus neutralization assays described in the section below: (4) vNY1/vNY1—tail scarification (t.s) of v-NY-S at $1x10^7$ PFU/animal, followed by an i.m. boost 4 weeks later of $1x10^7$ PFU/animal of v-NY-S virus into the right hind limb; (5) vNY1/rS—tail scarification (t.s) of v-NY-S at $1x10^7$ PFU/animal, followed by an i.m. boost 4 weeks later of 5 μg recombinant spike protein (aa 14–1209) in 1% alhydrogel (Invivogen) into the right hind limb; and (6) vNY0.1(i.n.)/MVA1- intranasal infection (i.n.) of v-NY-S at $1x10^6$ PFU/animal, followed by an i.m. boost 4 weeks later of $1x10^7$ PFU/animal of MVA-S virus into the right hind limb. As immunization controls, PBS buffer was used as a placebo vaccine for both priming and boosting shots. Blood was collected from immunized mouse cheeks 4 weeks after priming and 2 weeks after boosting, as described previously [118, 119]. Sera were prepared from blood and saved at -80˚C until use.

Prime-boost immunization regimens in Syrian hamsters

Eight-week-old male and female Syrian hamsters were housed in the Animal Facility of Academia Sinica (Taipei, Taiwan) for at least 3 days prior to vaccination experiments. We used three regimens of two-dosage prime/boost immunization (depicted in Fig 2A): (1) MVA5/MVA1-

intramuscular (i.m.) inoculation of MVA-S in the right hind limb at $5x10^7$ PFU/animal, followed by an i.m. boost 4 weeks later of $1x10^7$ PFU/animal of MVA-S virus; (2) vNY1/MVA1-tail scarification (t.s) of v-NY-S at $1x10^7$ PFU/animal, followed by an i.m. boost 4 weeks later of $1x10^7$ PFU/animal of MVA-S virus into the right hind limb; and (3) vNY5/MVA1- t.s. of v-NY-S at $5x10^7$ PFU/animal, followed by an i.m. boost 4 weeks later of $1x10^7$ PFU/animal of MVA-S virus into right hind limb. As immunization controls, PBS buffer was used as a placebo vaccine for both priming and boosting shots. Blood was collected from immunized hamster gingival veins 4 weeks after priming and 2 weeks after boosting, as described previously [118, 119]. Sera was prepared from blood and saved at -80˚C until use.

Immunoblotting

To measure SARS-CoV-2 S protein expression in cells infected with recombinant viruses, BSC40 and BHK21 cells ($5x10^5$) were infected with v-NY-S and MVA-S, respectively, at an MOI of 5 PFU/cell and incubated for 12 h prior to cell harvesting. Cells were lysed with sample buffer and proteins were separated by sodium dodecyl sulfate-polyacrylamide gel electrophoresis (SDS-PAGE). Proteins were then transferred to nitrocellulose membranes (BioRad) using a wet transfer apparatus (Bio-Rad). The membranes were blocked in 5% non-fat milk solution at room temperature (r.t.) for 1 h and incubated overnight with SARS-CoV-2 spike S2 mouse mAb (GTX632604, 1:1000 dilution) at 4˚C. The blots were then washed three times with PBST (PBS containing 0.1% Tween-20), incubated at r.t. with HRP goat anti-mouse IgG Ab (31430, 1:20,000) for 1 h and developed using a Western Lightening Enhanced Chemiluminescence kit (PerkinElmer) according to the manufacturer's protocol.

To test reactivity of immunized mouse and hamster sera to SARS-CoV-2 spike protein, the extracellular domain of spike protein from residue 14 to 1209, consisting of S1 and S2 but without the transmembrane domain, was expressed in HEK 293 cells and subsequently purified. The purified spike protein contained human complex type glycans, and exists as a trimer in solution with an apparent molecular weight between 170 to 235 kDa on SDS-PAGE (monomer), and ~600 kDa (trimer) on Superose 6 size-exclusion chromatography. Purified spike protein (20 ng/well) was separated by SDS-PAGE, transferred to nitrocellulose membranes and blocked in 5% non-fat milk solution at r.t. as described above. The membrane was separated into multiple strips and each strip was incubated overnight with individual sera collected from immunized mice (1:100 dilution) or hamsters (1:50) at 4˚C. These blots were then washed three times with PBST, incubated at r.t. with HRP goat anti-mouse (31430, 1:20,000) or HRP goat anti-hamster (PA1-28823, 1:5,000) antibodies for 1 h at r.t. and then developed using a Western Lightning Enhanced Chemiluminescence kit (PerkinElmer) according to the manufacturer's protocol.

Flow cytometry analysis of cell-surface SARS-CoV-2 S protein expression

To detect spike protein expression on the surface of cells infected with MVA-S or v-NY-S, BSC40 and BHK21 cells ($5x10^5$) were infected with v-NY-S and MVA-S, respectively, at an MOI of 5 PFU/cell and incubated for 12 h, before being detached via treatment with 2 mM EDTA in PBS. Cells were incubated with SARS-CoV-2 anti-RBD antibody (40592-T62, 1:500) at 4˚C for 1 h. The cells were then washed with FACS buffer (PBS containing 2% FBS), stained with FITC-conjugated goat anti-Rabbit IgG Ab (F1262, 1:500) for 1 h at 4˚C, washed with FACS buffer and analyzed by flow cytometry (BD LSR-II, BD Biosciences).

To detect anti-spike antibody in the sera of immunized mice and hamsters, SF9 insect cells were infected with either wild type baculovirus (WT-BAC) or a recombinant baculovirus (S-BAC) that expressed a chimeric SARS-CoV-2 S-gp64 protein in which the transmembrane

and C-terminal regions of S protein were replaced by the transmembrane and C-terminal regions of baculovirus GP64 so that the S-gp64 fusion protein would be expressed on insect cell surfaces. These cells were cultured for 48 h before incubating with mouse (1:100 dilution) or hamster (1:20 dilution) serum in FACS buffer for 1 hour on ice. After two washes with FACS buffer, the cells were incubated with Cy5-Goat anti-mouse IgG Ab (115-175-146, 1:500) or FITC-Goat anti-hamster IgG Ab (11-4211-85, 1:100) for 30 min on ice, washed twice, resuspended in FACS buffer containing propidium iodide, and then analyzed by flow cytometry (BD LSR-II).

SARS-CoV-2 pseudotyped virus neutralization assay

Lentiviral vectors pseudotyped with spike protein of wild type SARS-CoV-2 and SARS-CoV-2 variants of concern (VOC) (Table 2) were generated and titered by the National RNA Technology Platform and Gene Manipulation Core, Academia Sinica, Taipei, Taiwan. Neutralization assays on pseudotyped virus were performed by the same core facility as described previously [120], but with minor modifications. In brief, 1,000 units of the pseudotyped lentivirus with SARS-CoV-2 S protein were incubated at 37˚C for 1 h with serially-diluted sera obtained from vaccinated animals. The mixture was then added to HEK-293T cells expressing human ACE2 receptor (10^4 cells/well of a 96-well plate) and incubated for 24 h at 37˚C. This cell culture was then replaced with 100 μl of fresh DMEM plus 10% FBS, and the cells were incubated for another 48 h before undergoing luciferase assay. The reciprocal dilution of serum required for 50% inhibition of virus infection (ND_{50}) was assessed by measuring luciferase intensity.

SARS-CoV-2 neutralization assay

Serially diluted antibodies from immunized mice or hamsters were incubated at 37˚C for 1 h with 100 $TCID_{50}$ SARS-CoV-2 TCDC#4 (hCoV-19/Taiwan/4/2020). The mixtures were then added to pre-seeded Vero E6 cells for a 4-day incubation. Cells were fixed with 10% formaldehyde and stained with 0.5% crystal violet for 20 min. The plates were washed with tap water and scored for infection. The 50% protective titer was calculated according to the Reed & Muench Method [121].

Immunoglobulin ELISA for SARS-CoV-2 S-specific antibodies

Immunoglobulin ELISA was performed as described previously [17] with some modifications. Recombinant SARS-CoV-2 S protein (10 ng/well) was coated onto a 96-well plate (Costar assay plate, Corning, 3369) for 24 h at 4˚C. The plates were then washed with PBST and blocked with 1% BSA in PBS solution for 1 h, followed by washes with PBST. Coated plates

Table 2. SARS-CoV-2 variants of concern.

Scientific name	WHO label*	Mutation(s) in Spike protein (mutations in the RBD are in red)	Note
Wild Type (Wuhan-Hu-1 isolate)		NA	NC_045512.2
B.1.1.7	Alpha	69–70 del, Y144 del, N501Y, A570D, D614G, P681H, T716I, S982A, D1118H	VOC
B.1.351(501Y.V2)	Beta	L18F, D80A, D215G, 242–244 del, R246I, K417N, E484K, N501Y, D614G, A701V	VOC
P.1	Gamma	L18F, T20N, P26S, D138Y, R190S, K417T, E484K, N501Y, D614G, H655Y, T1027I	VOC
B.1.617		G142D, E154K, L452R, E484Q, D614G, P681R, Q1071H, H1101D	-
B.1.617.2	Delta	T19R, G142D, 156–157 del, R158G, L452R, T478K, D614G, P681R, D950N	VOC

* https://www.who.int/en/activities/tracking-SARS-CoV-2-variants/. RBD- receptor binding domain; VOC- variant of concern.

https://doi.org/10.1371/journal.pone.0257191.t002

were incubated for 1 h at r.t. with sera that had been serially diluted in PBS containing 1% BSA, then washed with PBST, and incubated with HRP-conjugated IgG2C (PA1-29288, 1:15000) or HRP-conjugated IgG1 (PA1-74421, 1:6000) secondary antibodies at r.t. for 1 h. Plates were washed with 5x PBST and incubated with commercial TMB substrate for color development (Clinical Science Products Inc.). To stop the reaction, 2N H_2SO_4 was added and the plates were read at an optical density of 450 nm using an ELISA reader. End-point titers were calculated as the serum dilutions that emitted an optical density (O.D) greater than four times the background level (secondary antibody only), as described previously [17].

ELISpot assay of mouse splenocytes

ELISpot assays to monitor cytokine levels in splenocytes stimulated with a SARS-CoV-2 spike peptide pool were performed essentially as described previously [109, 122]. In brief, spleens were collected from immunized mice four weeks after vaccine boosting. We mixed $4x10^5$ splenocytes with a peptide pool of SARS-CoV-2 S protein sequences (Miltenyi Biotech, 130-126-700) at 1 μg/ml concentration in 100 μl medium (RPMI + 10% FBS + 1% PS), and then incubated them for 24 h at 37˚C in ELISpot plates (MABTECH) precoated with IFN-γ (3321-4AST-2), IL-2 (3441-4APW-2), IL-4 (3311-4APW-2), IL-6 (3361-4APW-2) or TNF-α (3511-4APW-2). Cells were then washed with 5x PBS and the ELISpots were developed according to the manufacturer's protocol and quantified using an AID vSpot machine.

Analyses of T effector memory (Tem) cells

Flow cytometric analyses of Tem cells were performed as described previously [16] with minor modifications. Splenocytes were isolated from immunized mice at 4 weeks after vaccine boosting. After depleting red blood cells with Ammonium-Chloride-Potassium (ACK) lysis buffer, splenocytes were stimulated with 1 μg/ml of a SARS-CoV-2 spike-specific peptide pool (Miltenyi Biotech, 130-126-700) in medium (RPMI + 10% FBS + 1% PS) for 2 h at 37˚C. The cells were subsequently washed twice with FACS buffer, and then incubated with an antibody cocktail including anti-CD3-PE/Cyanine7, anti-CD4-FITC, anti-CD8-Pacific blue, anti-CD44-PE and anti-CD62L-APC for 15 min on ice. The cells then underwent fluorescence-activated cell sorting (FACS) analyses, whereby $CD4^+$ or $CD8^+$ subpopulations were first gated from total splenocytes, and then further gated for $CD44^+CD62L^-$ as Tem cells. Dead cells were stained with eFluor 506 viability dye (eBioscience). Cells were acquired using a BD LSR II (BD Biosciences) flow cytometer and data analyses were performed with FlowJo 8.7 software.

Syrian hamster challenge experiments

Syrian hamsters were immunized according to one of the three prime-boost vaccination regimens described above, anesthetized, with Zoletil-50 (50mg/kg) and then intranasally (i.n) challenged with $1x10^5$ PFU of SARS-CoV-2 TCDC#4 (hCoV-19/Taiwan/4/2020, GISAID accession ID: EPI_ISL_411927) (lot: IBMS20200819, $8x10^5$ PFU/ml) in a volume of 125 μl. All animals were weighed daily after SARS-CoV-2 challenge. At 3 and 7 days post infection (d.p.i.), lungs were harvested for SARS-CoV-2 virus titer determination, viral RNA quantification and histopathological examination. Differences in body weight between experimental groups of animals were analyzed statistically using a two-tailed unpaired Student's *t* test.

Quantification of viral titers in lung tissues by cell culture infection assay

The middle, inferior, and post-caval lobes of hamsters at 3 and 7 days post challenge with SARS-CoV-2 were homogenized in 4ml of DMEM with 2% FBS and 1% PS using a

homogenizer. Tissue homogenate was centrifuged at 15,000 rpm for 5 min and the supernatant was collected for live virus titration. Briefly, 10-fold serial dilutions of each sample were added in quadruplicate onto a Vero E6 cell monolayer and incubated for 4 days. Cells were then fixed with 10% formaldehyde and stained with 0.5% crystal violet for 20 min. The plates were washed with tap water and scored for infection. The fifty-percent tissue culture infectious dose ($TCID_{50}$)/ml was calculated according to the Reed & Muench Method [121].

Real-time RT-PCR for SARS-CoV-2 RNA quantification

To measure the RNA levels of SARS-CoV-2, specific primers targeting nucleotides 26,141 to 26,253 of the SARS-CoV-2 envelope (E) gene were used for real-time RT-PCR, as described previously [123], forward primer E-Sarbeco-F1 (5′-ACAGGTACGTTAATAGTTAATAGCGT-3′), reverse primer E-Sarbeco-R2 (5′-ATATTGCAGCAGTACGCACACA-3′), probe E-Sarbeco-P1 (5′-FAM-ACACTAGCCATCCTTACTGCGCTTCG-BBQ-3′). A total of 30 μl RNA solution was collected from each sample using an RNeasy Mini Kit (QIAGEN, Germany) according to the manufacturer's instructions. RNA sample (5 μl) was added into a total 25-μl mixture of the Superscript III one-step RT-PCR system with Platinum Taq Polymerase (Thermo Fisher Scientific, USA). The final reaction mix contained 400 nM of the forward and reverse primers, 200 nM probe, 1.6 mM deoxy-ribonucleoside triphosphate (dNTP), 4 mM magnesium sulfate, 50 nM ROX reference dye, and 1 μl of the enzyme mixture. Cycling conditions were performed using a one-step PCR protocol: 55˚C for 10 min for first-strand cDNA synthesis, followed by 3 min at 94˚C and 45 amplification cycles at 94˚C for 15 sec and 58˚C for 30 sec. Data was assessed using an Applied Biosystems 7500 Real-Time PCR System (Thermo Fisher Scientific). A synthetic 113-basepair oligonucleotide fragment was used as a qPCR standard to estimate copy numbers of the viral genome. The oligonucleotides were synthesized by Genomics BioSci & Tech Co. Ltd. (Taipei, Taiwan).

Histopathology

The left lung of each hamster at 3 and 7 days post challenge with SARS-CoV-2 was removed and fixed in 4% paraformaldehyde for 1 week. The lung samples were then embedded, sectioned, and stained with Hematoxylin and Eosin (H&E), followed by microscopic examination. Immunohistochemical staining was performed with a monoclonal rabbit anti-SARS-CoV/SARS-CoV-2 nucleocapsid (NP) antibody (1:1000, 40143-R001, Sino Biological), followed by incubation with Dako EnVision+ System HRP. Brownish signals were subsequently developed upon addition of 3,3' diaminobenzidine (DAB) and counterstained with hematoxylin. Images were photographed using a Zeiss Axioimager-Z1 microscope with 4x and 20x objective lenses.

Statistical analyses

Statistical analyses were conducted using Student's *t* test in Prism (version 9) software (GraphPad). For multiple comparisons, the p values were adjusted by the "fdr" method using the "p.adjust" function in R v4.0.4. Adjusted p values <0.05 were considered statistically significant. $^{*}p<0.05$; $^{**}p<0.01$; $^{***}p<0.001$; $^{****}p<0.0001$.

Supporting information

S1 Fig. Weight change in C57BL/6 mice after immunization with one of three regimens.
(TIF)

S2 Fig. (A). Images of skin scarification in Syrian hamsters at days 5,10 and 15 after primary immunization. (B) Weight change in Syrian hamsters after immunization with one of the three regimens.
(TIF)

S3 Fig. $TCID_{50}$ value of SARS-CoV-2 in lung tissues of hamsters at 7 d.p.i after SARS-CoV-2 challenge: PBS/PBS control (n = 3); MVA5/MVA1 (n = 5), the dotted line represents assay limits of detection.
(TIF)

S1 Raw images.
(PDF)

Acknowledgments

We thank Sue-Ping Lee of the Imaging Core Facility, Ya-Min Lin of the FACS Core Facility and Kun-Hai Yeh of Bioinformatics Core facility at the Institute of Molecular Biology and Data Science Statistical Cooperation Center-Statistical Clinics at Acadmia Sinica. We also thank Brad Cleveland for advice and assistance with the v-NY vector.

Author Contributions

Conceptualization: Rakesh Kulkarni, Wen Chang.

Data curation: Yu-Chi Chou, Wen Chang.

Formal analysis: Rakesh Kulkarni.

Funding acquisition: Shiu-Lok Hu, Wen Chang.

Investigation: Rakesh Kulkarni, Wen-Ching Chen, Ying Lee, Chi-Fei Kao, Hsiu-Hua Ma, Jia-Tsrong Jan, Chun-Che Liao, Jian-Jong Liang, Hui-Ying Ko, Cheng-Pu Sun, Yin-Shoiou Lin, Yu-Chi Chou.

Methodology: Rakesh Kulkarni, Jia-Tsrong Jan, Chun-Che Liao, Jian-Jong Liang, Hui-Ying Ko, Yi-Ling Lin, Yu-Chi Chou, Wen Chang.

Project administration: Rakesh Kulkarni, Wen Chang.

Resources: Shiu-Lok Hu, Jia-Tsrong Jan, Yu-Chiuan Wang, Sung-Chan Wei, Che Ma, Yu-Chan Chao, Yu-Chi Chou, Wen Chang.

Supervision: Rakesh Kulkarni, Jia-Tsrong Jan, Yi-Ling Lin, Yu-Chi Chou, Wen Chang.

Validation: Rakesh Kulkarni, Jia-Tsrong Jan, Chun-Che Liao, Jian-Jong Liang, Hui-Ying Ko, Yi-Ling Lin, Yu-Chi Chou, Wen Chang.

Visualization: Rakesh Kulkarni, Chi-Fei Kao, Wen Chang.

Writing – original draft: Rakesh Kulkarni, Shiu-Lok Hu, Jia-Tsrong Jan, Yi-Ling Lin, Che Ma, Yu-Chan Chao, Yu-Chi Chou, Wen Chang.

Writing – review & editing: Rakesh Kulkarni, Shiu-Lok Hu, Wen Chang.

References

1. Zhou P, Yang XL, Wang XG, Hu B, Zhang L, Zhang W, et al. A pneumonia outbreak associated with a new coronavirus of probable bat origin. Nature. 2020; 579(7798):270–3.

2. Coronaviridae Study Group of the International Committee on Taxonomy of V. The species Severe acute respiratory syndrome-related coronavirus: classifying 2019-nCoV and naming it SARS-CoV-2. Nat Microbiol. 2020; 5(4):536–44. https://doi.org/10.1038/s41564-020-0695-z PMID: 32123347

3. Drosten C, Gunther S, Preiser W, van der Werf S, Brodt HR, Becker S, et al. Identification of a novel coronavirus in patients with severe acute respiratory syndrome. N Engl J Med. 2003; 348(20):1967–76.

4. Zaki AM, van Boheemen S, Bestebroer TM, Osterhaus AD, Fouchier RA. Isolation of a novel coronavirus from a man with pneumonia in Saudi Arabia. N Engl J Med. 2012; 367(19):1814–20. https://doi.org/10.1056/NEJMoa1211721 PMID: 23075143

5. Petersen E, Koopmans M, Go U, Hamer DH, Petrosillo N, Castelli F, et al. Comparing SARS-CoV-2 with SARS-CoV and influenza pandemics. Lancet Infect Dis. 2020; 20(9):e238–e44. https://doi.org/10.1016/S1473-3099(20)30484-9 PMID: 32628905

6. Chan JF, Kok KH, Zhu Z, Chu H, To KK, Yuan S, et al. Genomic characterization of the 2019 novel human-pathogenic coronavirus isolated from a patient with atypical pneumonia after visiting Wuhan. Emerg Microbes Infect. 2020; 9(1):221–36. https://doi.org/10.1080/22221751.2020.1719902 PMID: 31987001

7. Hu B, Guo H, Zhou P, Shi ZL. Characteristics of SARS-CoV-2 and COVID-19. Nat Rev Microbiol. 2020.

8. Shang J, Wan Y, Luo C, Ye G, Geng Q, Auerbach A, et al. Cell entry mechanisms of SARS-CoV-2. Proc Natl Acad Sci U S A. 2020; 117(21):11727–34. https://doi.org/10.1073/pnas.2003138117 PMID: 32376634

9. Yang J, Petitjean SJL, Koehler M, Zhang Q, Dumitru AC, Chen W, et al. Molecular interaction and inhibition of SARS-CoV-2 binding to the ACE2 receptor. Nat Commun. 2020; 11(1):4541.

10. Ke Z, Oton J, Qu K, Cortese M, Zila V, McKeane L, et al. Structures and distributions of SARS-CoV-2 spike proteins on intact virions. Nature. 2020; 588(7838):498–502.

11. Hoffmann M, Kleine-Weber H, Schroeder S, Kruger N, Herrler T, Erichsen S, et al. SARS-CoV-2 Cell Entry Depends on ACE2 and TMPRSS2 and Is Blocked by a Clinically Proven Protease Inhibitor. Cell. 2020; 181(2):271–80 e8.

12. Dai L, Gao GF. Viral targets for vaccines against COVID-19. Nat Rev Immunol. 2021; 21:73–81. https://doi.org/10.1038/s41577-020-00480-0 PMID: 33340022

13. Ju B, Zhang Q, Ge J, Wang R, Sun J, Ge X, et al. Human neutralizing antibodies elicited by SARS-CoV-2 infection. Nature. 2020; 584(7819):115–9.

14. Grifoni A, Sidney J, Zhang Y, Scheuermann RH, Peters B, Sette A. Candidate Targets for Immune Responses to 2019-Novel Coronavirus (nCoV): Sequence Homology- and Bioinformatic-Based Predictions. SSRN. 2020:3541361. https://doi.org/10.2139/ssrn.3541361 PMID: 32714104

15. Grifoni A, Sidney J, Zhang Y, Scheuermann RH, Peters B, Sette A. A Sequence Homology and Bioinformatic Approach Can Predict Candidate Targets for Immune Responses to SARS-CoV-2. Cell Host Microbe. 2020; 27(4):671–80 e2.

16. Zhang NN, Li XF, Deng YQ, Zhao H, Huang YJ, Yang G, et al. A Thermostable mRNA Vaccine against COVID-19. Cell. 2020; 182(5):1271–83 e16.

17. Corbett KS, Edwards DK, Leist SR, Abiona OM, Boyoglu-Barnum S, Gillespie RA, et al. SARS-CoV-2 mRNA vaccine design enabled by prototype pathogen preparedness. Nature. 2020; 586(7830):567–71. https://doi.org/10.1038/s41586-020-2622-0 PMID: 32756549

18. Vogel AB, Kanevsky I, Che Y, Swanson KA, Muik A, Vormehr M, et al. BNT162b vaccines protect rhesus macaques from SARS-CoV-2. Nature. 2021.

19. Mercado NB, Zahn R, Wegmann F, Loos C, Chandrashekar A, Yu J, et al. Single-shot Ad26 vaccine protects against SARS-CoV-2 in rhesus macaques. Nature. 2020; 586(7830):583–8.

20. Logunov DY, Dolzhikova IV, Zubkova OV, Tukhvatulin AI, Shcheblyakov DV, Dzharullaeva AS, et al. Safety and immunogenicity of an rAd26 and rAd5 vector-based heterologous prime-boost COVID-19 vaccine in two formulations: two open, non-randomised phase 1/2 studies from Russia. Lancet. 2020; 396(10255):887–97. https://doi.org/10.1016/S0140-6736(20)31866-3 PMID: 32896291

21. van Doremalen N, Lambe T, Spencer A, Belij-Rammerstorfer S, Purushotham JN, Port JR, et al. ChAdOx1 nCoV-19 vaccine prevents SARS-CoV-2 pneumonia in rhesus macaques. Nature. 2020; 586(7830):578–82. https://doi.org/10.1038/s41586-020-2608-y PMID: 32731258

22. Krammer F. SARS-CoV-2 vaccines in development. Nature. 2020; 586(7830):516–27.

23. Klasse PJ, Nixon DF, Moore JP. Immunogenicity of clinically relevant SARS-CoV-2 vaccines in nonhuman primates and humans. Sci Adv. 2021; 7(12). https://doi.org/10.1126/sciadv.abe8065 PMID: 33608249

24. Greinacher A, Thiele T, Warkentin TE, Weisser K, Kyrle PA, Eichinger S. Thrombotic Thrombocytopenia after ChAdOx1 nCov-19 Vaccination. N Engl J Med. 2021.

25. Parrino J, Graham BS. Smallpox vaccines: Past, present, and future. J Allergy Clin Immunol. 2006; 118(6):1320–6.

26. Mayr A. Smallpox vaccination and bioterrorism with pox viruses. Comp Immunol Microbiol Infect Dis. 2003; 26(5–6):423–30.

27. Kreijtz JH, Goeijenbier M, Moesker FM, van den Dries L, Goeijenbier S, De Gruyter HL, et al. Safety and immunogenicity of a modified-vaccinia-virus-Ankara-based influenza A H5N1 vaccine: a randomised, double-blind phase 1/2a clinical trial. Lancet Infect Dis. 2014; 14(12):1196–207.

28. Verheust C, Goossens M, Pauwels K, Breyer D. Biosafety aspects of modified vaccinia virus Ankara (MVA)-based vectors used for gene therapy or vaccination. Vaccine. 2012; 30(16):2623–32.

29. Thompson M, Heath SL, Sweeton B, Williams K, Cunningham P, Keele BF, et al. DNA/MVA Vaccination of HIV-1 Infected Participants with Viral Suppression on Antiretroviral Therapy, followed by Treatment Interruption: Elicitation of Immune Responses without Control of Re-Emergent Virus. PLoS One. 2016; 11(10):e0163164.

30. Koch T, Dahlke C, Fathi A, Kupke A, Krahling V, Okba NMA, et al. Safety and immunogenicity of a modified vaccinia virus Ankara vector vaccine candidate for Middle East respiratory syndrome: an open-label, phase 1 trial. Lancet Infect Dis. 2020; 20(7):827–38. https://doi.org/10.1016/S1473-3099(20)30248-6 PMID: 32325037

31. Jacobs BL, Langland JO, Kibler KV, Denzler KL, White SD, Holechek SA, et al. Vaccinia virus vaccines: past, present and future. Antiviral Res. 2009; 84(1):1–13. https://doi.org/10.1016/j.antiviral.2009.06.006 PMID: 19563829

32. Walsh SR, Dolin R. Vaccinia viruses: vaccines against smallpox and vectors against infectious diseases and tumors. Expert Rev Vaccines. 2011; 10(8):1221–40. https://doi.org/10.1586/erv.11.79 PMID: 21854314

33. Verardi PH, Titong A, Hagen CJ. A vaccinia virus renaissance: new vaccine and immunotherapeutic uses after smallpox eradication. Hum Vaccin Immunother. 2012; 8(7):961–70. https://doi.org/10.4161/hv.21080 PMID: 22777090

34. Heo J, Reid T, Ruo L, Breitbach CJ, Rose S, Bloomston M, et al. Randomized dose-finding clinical trial of oncolytic immunotherapeutic vaccinia JX-594 in liver cancer. Nat Med. 2013; 19(3):329–36. https://doi.org/10.1038/nm.3089 PMID: 23396206

35. Zeh HJ, Downs-Canner S, McCart JA, Guo ZS, Rao UN, Ramalingam L, et al. First-in-man study of western reserve strain oncolytic vaccinia virus: safety, systemic spread, and antitumor activity. Mol Ther. 2015; 23(1):202–14. https://doi.org/10.1038/mt.2014.194 PMID: 25292189

36. Downs-Canner S, Guo ZS, Ravindranathan R, Breitbach CJ, O'Malley ME, Jones HL, et al. Phase 1 Study of Intravenous Oncolytic Poxvirus (vvDD) in Patients With Advanced Solid Cancers. Mol Ther. 2016; 24(8):1492–501.

37. Lauer UM, Schell M, Beil J, Berchtold S, Koppenhofer U, Glatzle J, et al. Phase I Study of Oncolytic Vaccinia Virus GL-ONC1 in Patients with Peritoneal Carcinomatosis. Clin Cancer Res. 2018; 24(18):4388–98. PMID: 29773661

38. Guo ZS, Lu B, Guo Z, Giehl E, Feist M, Dai E, et al. Vaccinia virus-mediated cancer immunotherapy: cancer vaccines and oncolytics. J Immunother Cancer. 2019; 7(1):6. https://doi.org/10.1186/s40425-018-0495-7 PMID: 30626434

39. Minev BR, Lander E, Feller JF, Berman M, Greenwood BM, Minev I, et al. First-in-human study of TK-positive oncolytic vaccinia virus delivered by adipose stromal vascular fraction cells. J Transl Med. 2019; 17(1):271.

40. Kennedy JS, Gurwith M, Dekker CL, Frey SE, Edwards KM, Kenner J, et al. Safety and immunogenicity of LC16m8, an attenuated smallpox vaccine in vaccinia-naive adults. J Infect Dis. 2011; 204(9):1395–402. https://doi.org/10.1093/infdis/jir527 PMID: 21921208

41. Garcia-Arriaza J, Garaigorta U, Perez P, Lazaro-Frias A, Zamora C, Gastaminza P, et al. COVID-19 vaccine candidates based on modified vaccinia virus Ankara expressing the SARS-CoV-2 spike induce robust T- and B-cell immune responses and full efficacy in mice. J Virol. 2021.

42. Liu R, Americo JL, Cotter CA, Earl PL, Erez N, Peng C, et al. One or two injections of MVA-vectored vaccine shields hACE2 transgenic mice from SARS-CoV-2 upper and lower respiratory tract infection. Proc Natl Acad Sci U S A. 2021; 118(12).

43. Routhu NK, Cheedarla N, Gangadhara S, Bollimpelli VS, Boddapati AK, Shiferaw A, et al. A modified vaccinia Ankara vector-based vaccine protects macaques from SARS-CoV-2 infection, immune pathology, and dysfunction in the lungs. Immunity. 2021; 54(3):542–56 e9. https://doi.org/10.1016/j.immuni.2021.02.001 PMID: 33631118

44. Cooney EL, Collier AC, Greenberg PD, Coombs RW, Zarling J, Arditti DE, et al. Safety of and immunological response to a recombinant vaccinia virus vaccine expressing HIV envelope glycoprotein. Lancet. 1991; 337(8741):567–72. https://doi.org/10.1016/0140-6736(91)91636-9 PMID: 1671940

45. Graham BS, Belshe RB, Clements ML, Dolin R, Corey L, Wright PF, et al. Vaccination of vaccinia-naive adults with human immunodeficiency virus type 1 gp160 recombinant vaccinia virus in a blinded, controlled, randomized clinical trial. The AIDS Vaccine Clinical Trials Network. J Infect Dis. 1992; 166 (2):244–52.

46. Cooney EL, McElrath MJ, Corey L, Hu SL, Collier AC, Arditti D, et al. Enhanced immunity to human immunodeficiency virus (HIV) envelope elicited by a combined vaccine regimen consisting of priming with a vaccinia recombinant expressing HIV envelope and boosting with gp160 protein. Proc Natl Acad Sci U S A. 1993; 90(5):1882–6.

47. Graham BS, Matthews TJ, Belshe RB, Clements ML, Dolin R, Wright PF, et al. Augmentation of human immunodeficiency virus type 1 neutralizing antibody by priming with gp160 recombinant vaccinia and boosting with rgp160 in vaccinia-naive adults. The NIAID AIDS Vaccine Clinical Trials Network. J Infect Dis. 1993; 167(3):533–7.

48. Sutter G, Moss B. Novel vaccinia vector derived from the host range restricted and highly attenuated MVA strain of vaccinia virus. Dev Biol Stand. 1995; 84:195–200.

49. Martin RM, Brady JL, Lew AM. The need for IgG2c specific antiserum when isotyping antibodies from C57BL/6 and NOD mice. J Immunol Methods. 1998; 212(2):187–92.

50. Liew FY. TH1 and TH2 cells: a historical perspective. Nature Reviews Immunology. 2002; 2(1):55–60.

51. Mosmann TR, Cherwinski H, Bond MW, Giedlin MA, Coffman RL. Two types of murine helper T cell clone. I. Definition according to profiles of lymphokine activities and secreted proteins. J Immunol. 1986; 136(7):2348–57.

52. Seder RA, Paul WE. Acquisition of lymphokine-producing phenotype by CD4+ T cells. Annu Rev Immunol. 1994; 12:635–73.

53. Roberts AD, Woodland DL. Cutting edge: effector memory CD8+ T cells play a prominent role in recall responses to secondary viral infection in the lung. J Immunol. 2004; 172(11):6533–7. PMID: 15153466

54. Sia SF, Yan LM, Chin AWH, Fung K, Choy KT, Wong AYL, et al. Pathogenesis and transmission of SARS-CoV-2 in golden hamsters. Nature. 2020; 583(7818):834–8.

55. Tostanoski LH, Wegmann F, Martinot AJ, Loos C, McMahan K, Mercado NB, et al. Ad26 vaccine protects against SARS-CoV-2 severe clinical disease in hamsters. Nat Med. 2020; 26(11):1694–700.

56. Imai M, Iwatsuki-Horimoto K, Hatta M, Loeber S, Halfmann PJ, Nakajima N, et al. Syrian hamsters as a small animal model for SARS-CoV-2 infection and countermeasure development. Proc Natl Acad Sci U S A. 2020; 117(28):16587–95. https://doi.org/10.1073/pnas.2009799117 PMID: 32571934

57. Yahalom-Ronen Y, Tamir H, Melamed S, Politi B, Shifman O, Achdout H, et al. A single dose of recombinant VSV-G-spike vaccine provides protection against SARS-CoV-2 challenge. Nat Commun. 2020; 11(1):6402. https://doi.org/10.1038/s41467-020-20228-7 PMID: 33328475

58. Rosenke K, Meade-White K, Letko M, Clancy C, Hansen F, Liu YN, et al. Defining the Syrian hamster as a highly susceptible preclinical model for SARS-CoV-2 infection. Emerg Microbes Infec. 2020; 9 (1):2673–84.

59. Baum A, Ajithdoss D, Copin R, Zhou A, Lanza K, Negron N, et al. REGN-COV2 antibodies prevent and treat SARS-CoV-2 infection in rhesus macaques and hamsters. Science. 2020; 370(6520):1110–5. https://doi.org/10.1126/science.abe2402 PMID: 33037066

60. Song Z, Bao L, Yu P, Qi F, Gong S, Wang J, et al. SARS-CoV-2 Causes a Systemically Multiple Organs Damages and Dissemination in Hamsters. Front Microbiol. 2020; 11:618891. https://doi.org/10.3389/fmicb.2020.618891 PMID: 33510731

61. Urata S, Maruyama J, Kishimoto-Urata M, Sattler RA, Cook R, Lin N, et al. Regeneration Profiles of Olfactory Epithelium after SARS-CoV-2 Infection in Golden Syrian Hamsters. ACS Chem Neurosci. 2021; 12(4):589–95. https://doi.org/10.1021/acschemneuro.0c00649 PMID: 33522795

62. Driouich JS, Cochin M, Lingas G, Moureau G, Touret F, Petit PR, et al. Favipiravir antiviral efficacy against SARS-CoV-2 in a hamster model. Nat Commun. 2021; 12(1):1735. https://doi.org/10.1038/s41467-021-21992-w PMID: 33741945

63. Brocato RL, Kwilas SA, Kim RK, Zeng X, Principe LM, Smith JM, et al. Protective efficacy of a SARS-CoV-2 DNA vaccine in wild-type and immunosuppressed Syrian hamsters. NPJ Vaccines. 2021; 6 (1):16.

64. Mohandas S, Yadav PD, Shete-Aich A, Abraham P, Vadrevu KM, Sapkal G, et al. Immunogenicity and protective efficacy of BBV152, whole virion inactivated SARS- CoV-2 vaccine candidates in the Syrian hamster model. iScience. 2021; 24(2):102054.

65. Munoz-Fontela C, Dowling WE, Funnell SGP, Gsell PS, Riveros-Balta AX, Albrecht RA, et al. Animal models for COVID-19. Nature. 2020; 586(7830):509–15.

66. Chan JF, Zhang AJ, Yuan S, Poon VK, Chan CC, Lee AC, et al. Simulation of the Clinical and Pathological Manifestations of Coronavirus Disease 2019 (COVID-19) in a Golden Syrian Hamster Model: Implications for Disease Pathogenesis and Transmissibility. Clin Infect Dis. 2020; 71(9):2428–46.

67. Lee AC, Zhang AJ, Chan JF, Li C, Fan Z, Liu F, et al. Oral SARS-CoV-2 Inoculation Establishes Subclinical Respiratory Infection with Virus Shedding in Golden Syrian Hamsters. Cell Rep Med. 2020; 1 (7):100121.

68. Bricker TL, Darling TL, Hassan AO, Harastani HH, Soung A, Jiang X, et al. A single intranasal or intramuscular immunization with chimpanzee adenovirus-vectored SARS-CoV-2 vaccine protects against pneumonia in hamsters. Cell Rep. 2021:109400.

69. Brustolin M, Rodon J, Rodriguez de la Concepcion ML, Avila-Nieto C, Cantero G, Perez M, et al. Protection against reinfection with D614- or G614-SARS-CoV-2 isolates in golden Syrian hamster. Emerg Microbes Infect. 2021; 10(1):797–809.

70. Osterrieder N, Bertzbach LD, Dietert K, Abdelgawad A, Vladimirova D, Kunec D, et al. Age-Dependent Progression of SARS-CoV-2 Infection in Syrian Hamsters. Viruses. 2020; 12(7).

71. Shaw RH, Stuart A, Greenland M, Liu X, Nguyen Van-Tam JS, Snape MD, et al. Heterologous prime-boost COVID-19 vaccination: initial reactogenicity data. Lancet. 2021; 397(10289):2043–6.

72. Lewis D. Mix-and-match COVID vaccines: the case is growing, but questions remain. Nature. 2021; 595(7867):344–5.

73. Callaway E. Mix-and-match COVID vaccines trigger potent immune response. Nature. 2021; 593 (7860):491.

74. Dhakal S, Ruiz-Bedoya CA, Zhou R, Creisher P, Villano J, Littlefield K, et al. Sex differences in lung imaging and SARS-CoV-2 antibody responses in a COVID-19 golden Syrian hamster model. bioRxiv. 2021.

75. Chan JFW, Zhang ANJX, Yuan SF, Poon VKM, Chan CCS, Lee ACY, et al. Simulation of the Clinical and Pathological Manifestations of Coronavirus Disease 2019 (COVID-19) in a Golden Syrian Hamster Model: Implications for Disease Pathogenesis and Transmissibility. Clin Infect Dis. 2020; 71 (9):2428–46.

76. Chung M, Bernheim A, Mei X, Zhang N, Huang M, Zeng X, et al. CT Imaging Features of 2019 Novel Coronavirus (2019-nCoV). Radiology. 2020; 295(1):202–7.

77. Ye Z, Zhang Y, Wang Y, Huang Z, Song B. Chest CT manifestations of new coronavirus disease 2019 (COVID-19): a pictorial review. Eur Radiol. 2020; 30(8):4381–9. https://doi.org/10.1007/s00330-020-06801-0 PMID: 32193638

78. Shi J, Wen Z, Zhong G, Yang H, Wang C, Huang B, et al. Susceptibility of ferrets, cats, dogs, and other domesticated animals to SARS-coronavirus 2. Science. 2020; 368(6494):1016–20. https://doi.org/10.1126/science.abb7015 PMID: 32269068

79. Rockx B, Kuiken T, Herfst S, Bestebroer T, Lamers MM, Oude Munnink BB, et al. Comparative pathogenesis of COVID-19, MERS, and SARS in a nonhuman primate model. Science. 2020; 368 (6494):1012–5. https://doi.org/10.1126/science.abb7314 PMID: 32303590

80. Rogers TF, Zhao F, Huang D, Beutler N, Burns A, He WT, et al. Isolation of potent SARS-CoV-2 neutralizing antibodies and protection from disease in a small animal model. Science. 2020.

81. Mokhtari T, Hassani F, Ghaffari N, Ebrahimi B, Yarahmadi A, Hassanzadeh G. COVID-19 and multiorgan failure: A narrative review on potential mechanisms. J Mol Histol. 2020; 51(6):613–28.

82. Zaim S, Chong JH, Sankaranarayanan V, Harky A. COVID-19 and Multiorgan Response. Curr Probl Cardiol. 2020; 45(8):100618. https://doi.org/10.1016/j.cpcardiol.2020.100618 PMID: 32439197

83. Francis ME, Goncin U, Kroeker A, Swan C, Ralph R, Lu Y, et al. SARS-CoV-2 infection in the Syrian hamster model causes inflammation as well as type I interferon dysregulation in both respiratory and non-respiratory tissues including the heart and kidney. PLoS Pathog. 2021; 17(7):e1009705. https://doi.org/10.1371/journal.ppat.1009705 PMID: 34265022

84. Poland GA, Ovsyannikova IG, Kennedy RB. SARS-CoV-2 immunity: review and applications to phase 3 vaccine candidates. Lancet. 2020; 396(10262):1595–606. https://doi.org/10.1016/S0140-6736(20)32137-1 PMID: 33065034

85. Corbett KS, Flynn B, Foulds KE, Francica JR, Boyoglu-Barnum S, Werner AP, et al. Evaluation of the mRNA-1273 Vaccine against SARS-CoV-2 in Nonhuman Primates. N Engl J Med. 2020; 383 (16):1544–55. https://doi.org/10.1056/NEJMoa2024671 PMID: 32722908

86. Tscherne A, Schwarz JH, Rohde C, Kupke A, Kalodimou G, Limpinsel L, et al. Immunogenicity and efficacy of the COVID-19 candidate vector vaccine MVA-SARS-2-S in preclinical vaccination. Proc Natl Acad Sci U S A. 2021; 118(28).

87. Tan AT, Linster M, Tan CW, Le Bert N, Chia WN, Kunasegaran K, et al. Early induction of functional SARS-CoV-2-specific T cells associates with rapid viral clearance and mild disease in COVID-19 patients. Cell Rep. 2021; 34(6):108728.

88. Walsh EE, Frenck RW Jr., Falsey AR, Kitchin N, Absalon J, Gurtman A, et al. Safety and Immunogenicity of Two RNA-Based Covid-19 Vaccine Candidates. N Engl J Med. 2020; 383(25):2439–50.

89. Guebre-Xabier M, Patel N, Tian JH, Zhou B, Maciejewski S, Lam K, et al. NVX-CoV2373 vaccine protects cynomolgus macaque upper and lower airways against SARS-CoV-2 challenge. Vaccine. 2020; 38(50):7892–6.

90. Mackett M, Smith GL, Moss B. Vaccinia virus: a selectable eukaryotic cloning and expression vector. Proc Natl Acad Sci U S A. 1982; 79(23):7415–9. https://doi.org/10.1073/pnas.79.23.7415 PMID: 6296831

91. Piccini A, Perkus ME, Paoletti E. Vaccinia virus as an expression vector. Methods Enzymol. 1987; 153:545–63. https://doi.org/10.1016/0076-6879(87)53077-4 PMID: 2828850

92. Folegatti PM, Ewer KJ, Aley PK, Angus B, Becker S, Belij-Rammerstorfer S, et al. Safety and immunogenicity of the ChAdOx1 nCoV-19 vaccine against SARS-CoV-2: a preliminary report of a phase 1/2, single-blind, randomised controlled trial. Lancet. 2020; 396(10249):467–78.

93. Ramasamy MN, Minassian AM, Ewer KJ, Flaxman AL, Folegatti PM, Owens DR, et al. Safety and immunogenicity of ChAdOx1 nCoV-19 vaccine administered in a prime-boost regimen in young and old adults (COV002): a single-blind, randomised, controlled, phase 2/3 trial. Lancet. 2021; 396 (10267):1979–93.

94. Hsieh CL, Goldsmith JA, Schaub JM, DiVenere AM, Kuo HC, Javanmardi K, et al. Structure-based design of prefusion-stabilized SARS-CoV-2 spikes. Science. 2020.

95. Li C, Chen YX, Liu FF, Lee AC, Zhao Y, Ye ZH, et al. Absence of vaccine-enhanced disease with unexpected positive protection against SARS-CoV-2 by inactivated vaccine given within three days of virus challenge in Syrian hamster model. Clin Infect Dis. 2021.

96. Hu SL, Plowman GD, Sridhar P, Stevenson US, Brown JP, Estin CD. Characterization of a recombinant vaccinia virus expressing human melanoma-associated antigen p97. J Virol. 1988; 62(1):176–80. https://doi.org/10.1128/JVI.62.1.176-180.1988 PMID: 3334743

97. Tartaglia J, Perkus ME, Taylor J, Norton EK, Audonnet JC, Cox WI, et al. NYVAC: a highly attenuated strain of vaccinia virus. Virology. 1992; 188(1):217–32.

98. Hu SL, Zarling JM, Chinn J, Travis BM, Moran PA, Sias J, et al. Protection of macaques against simian AIDS by immunization with a recombinant vaccinia virus expressing the envelope glycoproteins of simian type D retrovirus. Proc Natl Acad Sci U S A. 1989; 86(18):7213–7.

99. Thippeshappa R, Tian B, Cleveland B, Guo W, Polacino P, Hu SL. Oral Immunization with Recombinant Vaccinia Virus Prime and Intramuscular Protein Boost Provides Protection against Intrarectal Simian-Human Immunodeficiency Virus Challenge in Macaques. Clin Vaccine Immunol. 2015; 23 (3):204–12.

100. Seneschal J, Jiang XD, Kupper TS. Langerin(+) Dermal DC, but Not Langerhans Cells, Are Required for Effective CD8-Mediated Immune Responses after Skin Scarification with Vaccinia Virus. J Invest Dermatol. 2014; 134(3):686–94.

101. Phelps A, Gates AJ, Eastaugh L, Hillier M, Ulaeto DO. Comparative Efficacy of Intramuscular and Scarification Routes of Administration of Live Smallpox Vaccine in a Murine Challenge Model. Vaccine. 2017; 35(31):3889–96.

102. Xia S, Zhang Y, Wang Y, Wang H, Yang Y, Gao GF, et al. Safety and immunogenicity of an inactivated SARS-CoV-2 vaccine, BBIBP-CorV: a randomised, double-blind, placebo-controlled, phase 1/2 trial. Lancet Infect Dis. 2021; 21(1):39–51. https://doi.org/10.1016/S1473-3099(20)30831-8 PMID: 33069281

103. Ella R, Reddy S, Jogdand H, Sarangi V, Ganneru B, Prasad S, et al. Safety and immunogenicity of an inactivated SARS-CoV-2 vaccine, BBV152: interim results from a double-blind, randomised, multicentre, phase 2 trial, and 3-month follow-up of a double-blind, randomised phase 1 trial. Lancet Infect Dis. 2021.

104. Baden LR, El Sahly HM, Essink B, Kotloff K, Frey S, Novak R, et al. Efficacy and Safety of the mRNA-1273 SARS-CoV-2 Vaccine. New Engl J Med. 2021; 384(5):403–16. https://doi.org/10.1056/NEJMoa2035389 PMID: 33378609

105. Polack FP, Thomas SJ, Kitchin N, Absalon J, Gurtman A, Lockhart S, et al. Safety and Efficacy of the BNT162b2 mRNA Covid-19 Vaccine. N Engl J Med. 2020; 383(27):2603–15. https://doi.org/10.1056/NEJMoa2034577 PMID: 33301246

106. Zhang N, Li XF, Deng YQ, et al A thermostable mRNA vaccine against COVID-19. Cell. 2020: In Press. https://doi.org/10.1016/j.cell.2020.07.024 PMID: 32795413

107. Keech C, Albert G, Cho I, Robertson A, Reed P, Neal S, et al. Phase 1–2 Trial of a SARS-CoV-2 Recombinant Spike Protein Nanoparticle Vaccine. N Engl J Med. 2020; 383(24):2320–32. https://doi.org/10.1056/NEJMoa2026920 PMID: 32877576

108. Voysey M, Clemens SAC, Madhi SA, Weckx LY, Folegatti PM, Aley PK, et al. Safety and efficacy of the ChAdOx1 nCoV-19 vaccine (AZD1222) against SARS-CoV-2: an interim analysis of four randomised controlled trials in Brazil, South Africa, and the UK. Lancet. 2021; 397(10269):99–111. https://doi.org/10.1016/S0140-6736(20)32661-1 PMID: 33306989

109. Feng L, Wang Q, Shan C, Yang C, Feng Y, Wu J, et al. An adenovirus-vectored COVID-19 vaccine confers protection from SARS-COV-2 challenge in rhesus macaques. Nat Commun. 2020; 11 (1):4207. https://doi.org/10.1038/s41467-020-18077-5 PMID: 32826924

110. King RG, Silva-Sanchez A, Peel JN, Botta D, Meza-Perez S, Allie R, et al. Single-dose intranasal administration of AdCOVID elicits systemic and mucosal immunity against SARS-CoV-2 in mice. bioRxiv. 2020. https://doi.org/10.1101/2020.10.10.331348 PMID: 33052351

111. Zarling JM, Eichberg JW, Moran PA, McClure J, Sridhar P, Hu SL. Proliferative and cytotoxic T cells to AIDS virus glycoproteins in chimpanzees immunized with a recombinant vaccinia virus expressing AIDS virus envelope glycoproteins. J Immunol. 1987; 139(4):988–90. PMID: 3497202

112. Hu SL, Travis BM, Garrigues J, Zarling JM, Sridhar P, Dykers T, et al. Processing, Assembly, and Immunogenicity of Human-Immunodeficiency-Virus Core Antigens Expressed by Recombinant Vaccinia Virus. Virology. 1990; 179(1):321–9. https://doi.org/10.1016/0042-6822(90)90300-g PMID: 2219727

113. Wyatt LS, Earl PL, Moss B. Generation of Recombinant Vaccinia Viruses. Curr Protoc Microbiol. 2015; 39:14A 4 1–A 4 8. https://doi.org/10.1002/9780471729259.mc14a04s39 PMID: 26528782

114. Cotter CA, Earl PL, Wyatt LS, Moss B. Preparation of Cell Cultures and Vaccinia Virus Stocks. Curr Protoc Microbiol. 2015; 39:14A 3 1–A 3 8. https://doi.org/10.1002/9780471729259.mc14a03s39 PMID: 26528781

115. Chakrabarti S, Brechling K, Moss B. Vaccinia virus expression vector: coexpression of beta-galactosidase provides visual screening of recombinant virus plaques. Mol Cell Biol. 1985; 5(12):3403–9. https://doi.org/10.1128/mcb.5.12.3403-3409.1985 PMID: 3939316

116. Kasani SK, Cheng HY, Yeh KE, Chang SJ, Hsu PW, Tung SY, et al. Reply to "Bioinformatics Analysis of Differential Innate Immune Signaling in Macrophages by Wild-Type Vaccinia Mature Virus and a Mutant Virus with a Deletion of the A26 Protein". J Virol. 2017; 91(24). https://doi.org/10.1128/JVI.01600-17 PMID: 29191985

117. Izmailyan R, Hsao JC, Chung CS, Chen CH, Hsu PW, Liao CL, et al. Integrin beta1 mediates vaccinia virus entry through activation of PI3K/Akt signaling. J Virol. 2012; 86(12):6677–87. https://doi.org/10.1128/JVI.06860-11 PMID: 22496232

118. Golde WT, Gollobin P, Rodriguez LL. A rapid, simple, and humane method for submandibular bleeding of mice using a lancet. Lab Animal. 2005; 34(9):39–43. https://doi.org/10.1038/laban1005-39 PMID: 16195737

119. Rodrigues MV, de Castro SO, de Albuquerque CZ, Mattaraia VGD, Santoro ML. The gingival vein as a minimally traumatic site for multiple blood sampling in guinea pigs and hamsters. Plos One. 2017; 12 (5). https://doi.org/10.1371/journal.pone.0177967 PMID: 28531179

120. Kuo TY, Lin MY, Coffman RL, Campbell JD, Traquina P, Lin YJ, et al. Development of CpG-adjuvanted stable prefusion SARS-CoV-2 spike antigen as a subunit vaccine against COVID-19. Sci Rep. 2020; 10(1):20085. https://doi.org/10.1038/s41598-020-77077-z PMID: 33208827

121. Ramakrishnan MA. Determination of 50% endpoint titer using a simple formula. World J Virol. 2016; 5 (2):85–6. https://doi.org/10.5501/wjv.v5.i2.85 PMID: 27175354

122. Haun BK, Lai CY, Williams CA, Wong TAS, Lieberman MM, Pessaint L, et al. CoVaccine HT Adjuvant Potentiates Robust Immune Responses to Recombinant SARS-CoV-2 Spike S1 Immunization. Front Immunol. 2020; 11:599587. https://doi.org/10.3389/fimmu.2020.599587 PMID: 33193454

123. Corman VM, Landt O, Kaiser M, Molenkamp R, Meijer A, Chu DK, et al. Detection of 2019 novel coronavirus (2019-nCoV) by real-time RT-PCR. Euro Surveill. 2020; 25(3).